Targeting of the Arf-GEF GBF1 to lipid droplets and Golgi membranes

S. Bouvet, M.-P. Golinelli-Cohen, V. Contremoulins, C. L Jackson

Targeting of the Arf-GEF GBF1 to lipid droplets and Golgi membranes

Samuel Bouvet[1,2], Marie-Pierre Golinelli-Cohen[1,*], Vincent Contremoulins[1,3] and Catherine L. Jackson[1,2,‡]

[1]Institut Jacques Monod, CNRS, UMR 7592, Université Paris Diderot, Sorbonne Paris Cité, F-75205 Paris, France
[2]Membrane Dynamics and Intracellular Trafficking, Institut Jacques Monod, Paris, France
[3]ImagoSeine BioImaging Core Facility, Institut Jacques Monod, Paris, France

*Present address: Institut de Chimie des Substances Naturelles, CNRS UPR2301, 91190, Gif-sur-Yvette, France
‡Author for correspondence (jackson@ijm.univ-paris-diderot.fr)

Accepted 16 July 2013
Journal of Cell Science 126, 4794–4805

doi: 10.1242/jcs.134254

Summary

Lipid droplet metabolism and secretory pathway trafficking both require activation of the Arf1 small G protein. The spatiotemporal regulation of Arf1 activation is mediated by guanine nucleotide exchange factors (GEFs) of the GBF and BIG families, but the mechanisms of their localization to multiple sites within cells are poorly understood. Here we show that GBF1 has a lipid-binding domain (HDS1) immediately downstream of the catalytic Sec7 domain, which mediates association with both lipid droplets and Golgi membranes in cells, and with bilayer liposomes and artificial droplets *in vitro*. An amphipathic helix within HDS1 is necessary and sufficient for lipid binding, both *in vitro* and in cells. The HDS1 domain of GBF1 is stably associated with lipid droplets in cells, and the catalytic Sec7 domain inhibits this potent lipid-droplet-binding capacity. Additional sequences upstream of the Sec7 domain–HDS1 tandem are required for localization to Golgi membranes. This mechanism provides insight into crosstalk between lipid droplet function and secretory trafficking.

Key words: Lipid droplet, Arf1 small G protein, Lipid binding domain, Golgi, Amphipathic helix, Guanine nucleotide exchange factor (GEF)

Introduction

Organelle identity is maintained dynamically by specific recruitment of proteins to membranes of a characteristic lipid composition. In many cases, an organelle is defined by a combination of a rare lipid and specific proteins, most commonly phosphoinositides and activated small G proteins (Behnia and Munro, 2005). This combination allows peripheral proteins such as protein coats, lipid modifying enzymes and actin cytoskeleton regulators to associate specifically with each compartment and contribute to their functioning and maturation. Although small G proteins such as Arf1 and Rab1 are known to function in recruiting proteins to membranes of the early secretory pathway (Gillingham and Munro, 2007), these membranes lack a characteristic phosphorylated phosphoinositide to confer compartment identity. Instead, other signature features of these compartments are used as targeting information, such as lipid packing defects, that are sensed by a specific class of amphipathic helices (Bigay and Antonny, 2012; Vamparys et al., 2013; Vanni et al., 2013).

Lipid droplets (LDs), the major energy storage depots of eukaryotic cells, are now recognized as bona fide organelles that interface with membrane trafficking pathways (Liu et al., 2004; Walther and Farese, 2012). They are distinct from other organelles in having a neutral lipid core surrounded by a phospholipid monolayer rather than a bilayer encompassing an aqueous interior. However, the composition of the phospholipids encircling LDs shares features with that of early secretory pathway membranes, notably its lack of a specific phosphorylated phosphoinositide as a compartment marker (Bartz et al., 2007a). In addition to triglycerides, which are the major energy storage molecules of eukaryotic cells, the neutral lipid core of LDs also contains esterified cholesterol. These two classes of neutral lipids serve as storage precursors of the two major lipid components of cellular membranes. In yeast, it has been shown that trafficking through the secretory pathway is coordinated with storage of neutral lipids in LDs, probably to provide the cell with the capacity to respond rapidly to demands for new membrane synthesis when growth is stimulated, and to channel newly synthesized membrane precursors from the ER to LDs for storage when growth is inhibited (Gaspar et al., 2011; Gaspar et al., 2008).

The metabolism of LDs has received considerable attention in recent years because of their central role in metabolic diseases, notably lipodystrophies and obesity (Walther and Farese, 2012; Zechner et al., 2012). Obesity is a particularly serious health concern because of its prevalence, and its predisposition to serious illnesses such as diabetes, fatty liver disease, heart disease and cancer (Bozza and Viola, 2010; Cohen et al., 2011; Greenberg et al., 2011). LDs are also required for the infectious cycle of pathogens such as hepatitis C virus, Dengue virus and *Chlamydia*, which target fat metabolic cells and/or lipid metabolic pathways for their propagation (Saka and Valdivia, 2012; Stehr et al., 2012).

Both the mechanisms linking LDs to the secretory pathway, and targeting of proteins to the LD surface are poorly understood. We and others have identified a crucial role of the Arf1 small G protein and its regulators in recruitment of LD-associated proteins to the LD surface, a function that is evolutionarily

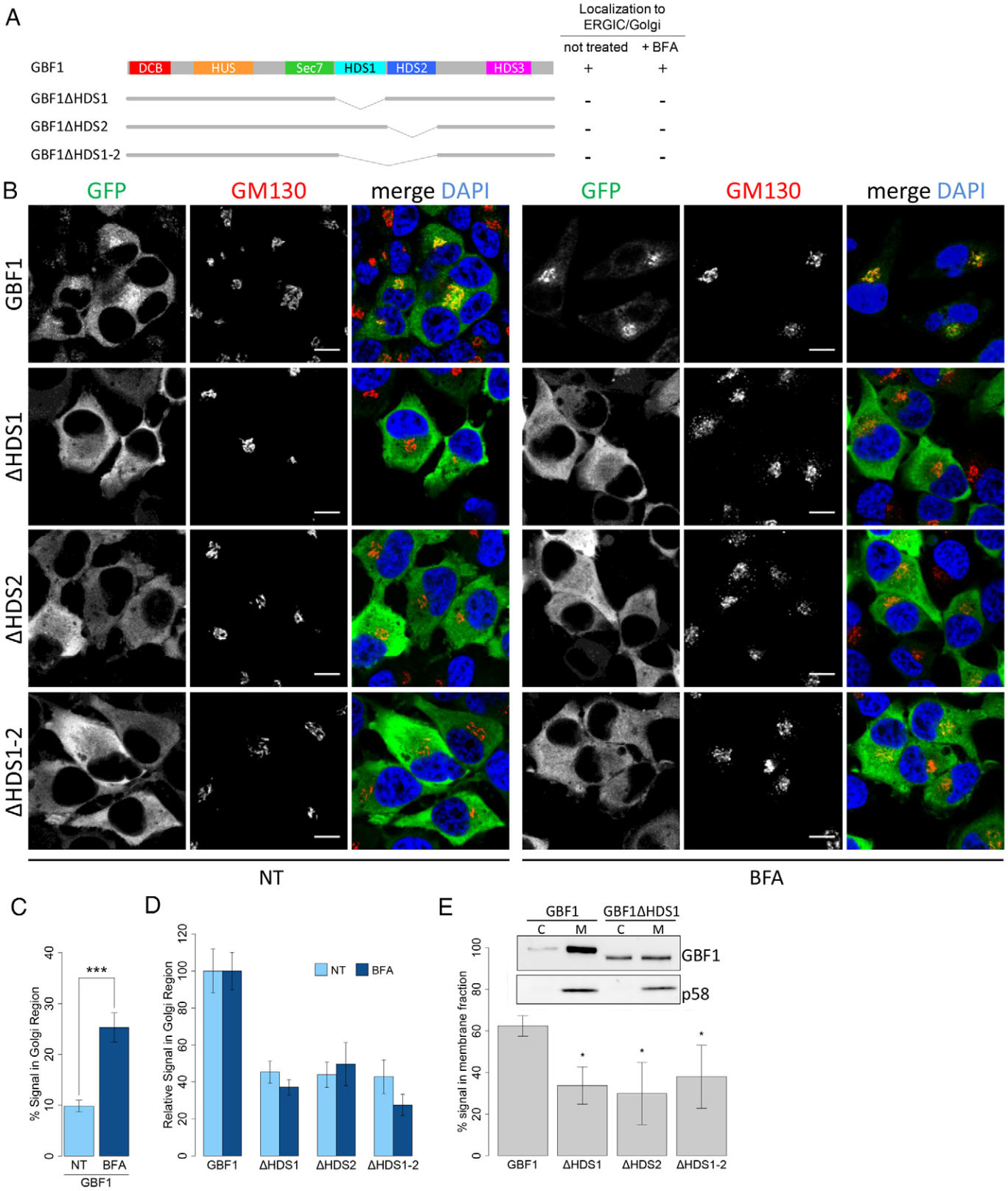

Fig. 1 See next page for legend.

Fig. 1. The C-terminal HDS1 and HDS2 domains are required for GBF1 association with ERGIC and Golgi membranes in cells. (A) Schematic diagram of GBF1 showing homology domains and deletion constructs (left panel), and summary of localization results (right panel). (B) HeLa cells expressing the indicated GFP-GBF1 construct were treated with 10 μg/ml BFA (BFA) or DMSO alone (NT, not treated) for 10 minutes at 37℃. Cells were then fixed and immunostained for Golgi colocalization as described in Materials and Methods. Scale bars: 10 μm. (C,D) Quantification of experiments shown in B. Localization of wild-type GBF1 (C) or GBF1 deletion mutants (D) in the Golgi region was calculated as described in Materials and Methods. In D, values were normalized against wild-type GBF1. $***P<10^{-10}$ (Standard *t*-test); (E) HeLa cells expressing the indicated GFP-GBF1 construct were incubated with 10 μg/ml BFA for 10 minutes at 37℃ before harvesting and fractionation. The blot shown is representative of at least three independent experiments. p58 (ERGIC53), is a marker of the membrane fraction. C, cytosolic fraction; M, membrane fraction. Band density was quantified using ImageJ (NIH) and the amount of membrane-bound protein was calculated as described in Materials and Methods. Error bars represent the 95% confidence interval. $*P<0.01$ (standard Student *t*-test).

conserved from *Drosophila* to humans (Beller et al., 2008; Guo et al., 2008; Soni et al., 2009). However, the mechanisms by which Arf1 and its regulators themselves are recruited to LDs are not well understood. In the secretory pathway, Arf1 is involved in recruitment of coats to membranes to form transport vesicles (Bonifacino and Lippincott-Schwartz, 2003). At the *cis*-Golgi, the Arf1 activator GBF1, a guanine nucleotide exchange factor (GEF) that switches Arf1 from its inactive GDP-bound to active GTP-bound form, recruits the COPI coat to membranes, the first step in formation of COPI-coated vesicles (Beck et al., 2009). At the *trans*-Golgi, Arf1 is activated by members of a distinct family of GEFs, the BIG/Sec7 family. The GBF and BIG GEFs are large proteins that share a common domain structure (Bui et al., 2009; Gillingham and Munro, 2007). Among these large Arf GEFs, the mechanism of recruitment of the BIG/Sec7 proteins is the best characterized. However, two distinct localization mechanisms involving direct interactions with the BIG GEF proteins have been demonstrated (Christis and Munro, 2012; Richardson et al., 2012). The HDS1 domain downstream of the catalytic domain of yeast Sec7p is necessary for binding to membranes in an Arf1-dependent manner, as part of a positive feedback loop enhancing membrane binding (Richardson et al., 2012). It has also been shown that the N-terminus of the mammalian and *Drosophila* homologue of Sec7p, BIG1, interacts with the small G protein Arl1, a *trans*-Golgi-localized protein, which mediates the specific recruitment of BIG1 to *trans*-Golgi membranes (Christis and Munro, 2012). How these two localization mechanisms are coordinated is not known. For the GBF family of GEFs, the N-terminal region of mammalian GBF1 has been shown to interact directly with Rab1, which contributes to its localization to the Golgi (Monetta et al., 2007). Here we show that two regions of GBF1, both the HDS1 domain and the N-terminus, are required for its Golgi localization, whereas the HDS1 domain alone is required for localization to LDs. We show that the HDS1 domain is a lipid-binding domain, which can associate both with bilayer liposomes and LDs, *in vitro* and in cells, through an amphipathic helix within the domain.

Results

The HDS1 and HDS2 domains of GBF1 are required for localization to both LDs and Golgi membranes

In cells under normal growth conditions, GBF1 localizes primarily to membranes of the early secretory pathway, including the *cis*-Golgi and the ER–Golgi intermediate compartment (ERGIC), cycling dynamically between membranes and cytosol (García-Mata et al., 2003; Niu et al., 2005; Zhao et al., 2006). We made the surprising observation that the HDS1 and HDS2 domains of GBF1 (shown schematically in Fig. 1A) localize to LDs, and not to the Golgi, when expressed on their own in cells treated with fatty acids (Ellong et al., 2011) (see also Fig. 3C). However, this result is consistent with the known role of GBF1 in LD metabolism, including localization of the full-length protein to LDs in fatty-acid-treated cells (Soni et al., 2009), and leads to two hypotheses: either HDS1 and HDS2 localize only to LDs, and other domains of GBF1 specifically target the protein to secretory pathway membranes, or HDS1 and HDS2 mediate localization to both sites in a regulated manner. To distinguish between these possibilities, we tested localization of GBF1 and deletions of HDS1, HDS2 or the two domains together (Fig. 1). Treatment of cells with the Arf1-GEF inhibitor brefeldin A (BFA) for 10–20 minutes leads to an increase in the amount of GBF1 on ERGIC elements and the Golgi, as determined by both fluorescence microscopy and fractionation (Niu et al., 2005; Szul et al., 2005; Zhao et al., 2006). As is the case for certain other peripherally associated Golgi proteins that cycle dynamically between membranes and cytosol, release from Golgi membranes occurs during the fractionation procedure (Panic et al., 2003), but for GBF1, treatment of cells with BFA prior to fractionation appears to protect this release from membranes, at least partially, resulting in ~60% of the protein remaining associated with the membrane fraction (supplementary material Fig. S1). In contrast, deletion of either the HDS1 or the HDS2 domain, or both together, resulted in a primarily cytosolic localization of the protein as assayed by fluorescence imaging (Fig. 1B–D) or subcellular fractionation (Fig. 1E). Quantification of fluorescence images demonstrated that the HDS1 and HDS2 deletion mutants were significantly delocalized from the perinuclear Golgi region, both in the absence and presence of BFA (Fig. 1B,C). Hence the HDS1 and HDS2 domains are required for GBF1 localization to ERGIC and Golgi membranes. Deletion of the entire C-terminal portion of GBF1 downstream of the catalytic Sec7 domain abolished the association of the protein with Golgi and ERGIC membranes, in the presence or absence of BFA, as monitored both by fluorescence microscopy and subcellular fractionation (supplementary material Fig. S2). However, truncations removing sequences downstream of the HDS1 and HDS2 domains all resulted in localization to membranes in both assays (supplementary material Fig. S2), indicating that no other regions of the GBF1 C-terminal region are required for membrane targeting. Hence the HDS1 and HDS2 domains of GBF1 are required both for localization to secretory pathway membranes and to LDs.

HDS1 is a lipid-binding domain

To determine the mechanism by which the HDS1 domain localizes to membranes, we purified HDS1 as a GST fusion from *Escherichia coli*, and tested binding to liposomes *in vitro* using a sucrose gradient flotation assay. We tested liposomes of different compositions, including a phospholipid mixture derived from soybeans called azolectin [~55% phosphatidylcholine (PC), 20% phosphatidylethanolamine (PE), and other less abundant phospholipid species], a mixture of phospholipids of composition similar to Golgi membranes ['Golgi mix': 50% egg

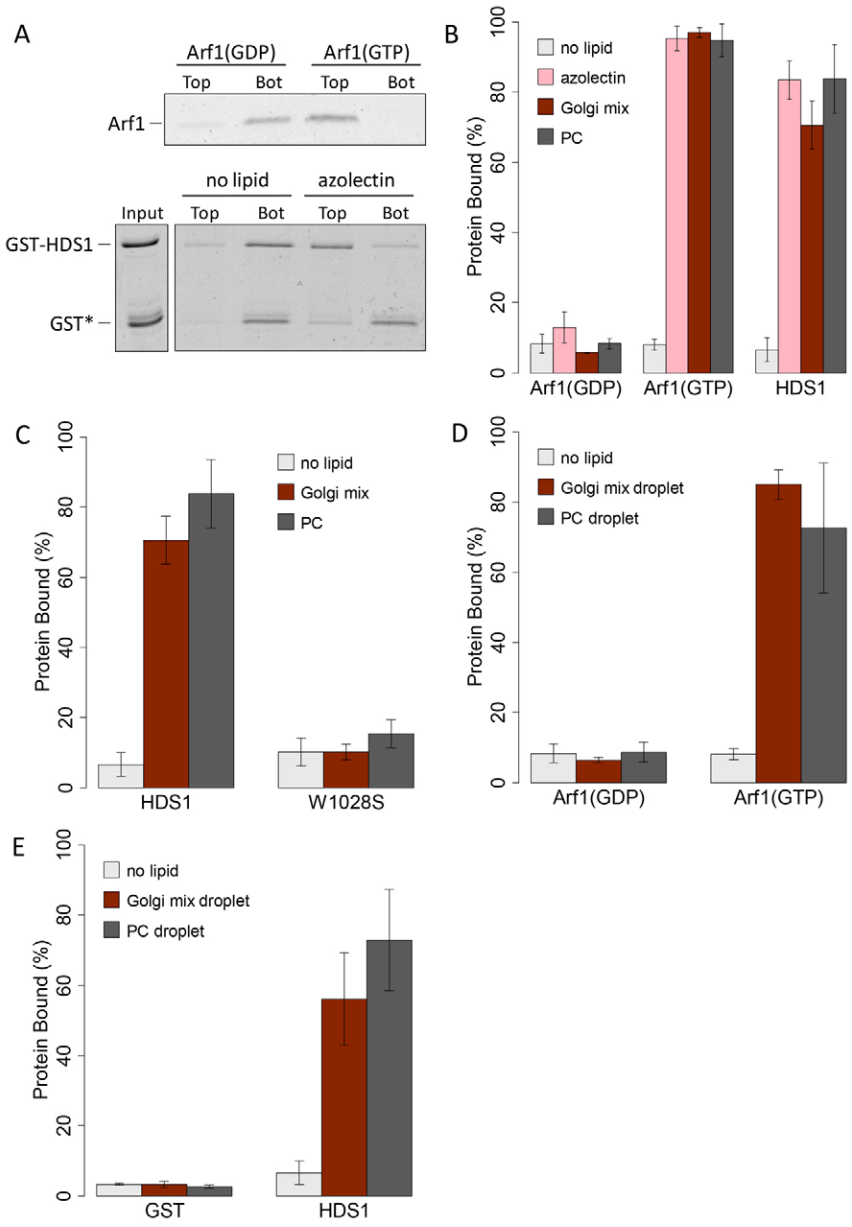

Fig. 2. HDS1 binds to liposomes and artificial droplets *in vitro*. (A) Myr-Arf1 loaded with GDP or with GTP (top panel), or GST–HDS1 (bottom panel), were incubated with or without azolectin liposomes at 37℃ for 30 minutes. Sucrose gradient flotations were performed as described in Materials and Methods. Top: top fraction. Bot: bottom fraction. (B,C) Sucrose gradient flotations were performed with azolectin liposomes (in B only), liposomes of defined composition similar to Golgi membranes (Golgi mix), egg PC liposomes (PC) or without liposomes (no lipid). The percentage bound protein is the ratio of protein in the top fraction to the sum of the intensities in the top and the bottom fractions, expressed as a percentage. W1028S indicates GST–HDS1 with the W1028S point mutation (GST–HDS1 W1028S). (D) Myr-Arf1 loaded with GDP or with GTP was incubated at 37℃ for 30 minutes with or without artificial droplets prepared using Golgi mix phospholipids (Golgi mix droplet) or egg PC (PC droplets). (E) GST or GST–HDS1 incubated as in D in the absence (no lipid) or in the presence of Golgi mix or PC droplets. Error bars represent the standard deviation of at least three independent experiments.

PC, 19% egg PE, 10% liver phosphatidylinositol (PI), 5% brain phosphatidylserine (PS), and 16% cholesterol, where the percentage given is a molar ratio] (Bigay et al., 2005) or pure egg PC. We found that the HDS1 domain showed a high level of binding to azolectin liposomes, to an extent approaching that of myristoylated Arf1–GTP (Fig. 2A,B). HDS1 also showed high levels of binding to Golgi mix liposomes, and to pure PC liposomes (Fig. 2B). A single point mutation of a highly conserved tryptophan residue (HDS1-W1028S, see below) severely inhibited liposome binding (Fig. 2C). These results indicate that HDS1 is a direct lipid-binding domain. Interestingly, the HDS1 domain of GBF1 is able to bind to liposomes containing only neutral lipids, and therefore does not have a requirement *in vitro* for charged or rare lipids (e.g. phosphorylated PIs). Furthermore, the GBF1 lipid-binding HDS1 domain does not require another protein, such as Arf1, to efficiently bind to liposomes, a property that differs from yeast Sec7p, which does require Arf1–GTP for lipid binding *in vitro* (Richardson et al., 2012). Hence, although GBF1 shares a similar domain structure with that of members of the BIG/Sec7 family of Arf GEFs (its HDS1 domain shares 23% identity and 45% similarity with that of yeast Sec7p), the two GEFs appear to differ in their requirement for Arf1 for lipid binding.

HDS1 binds to artificial droplets *in vitro*

We sought to test the ability of HDS1 to associate with artificial LDs *in vitro*, using a recently developed *in vitro* method to produce artificial droplets and assay protein binding by flotation analysis (see Materials and Methods). Artificial LDs can be formed by combining triglycerides and phospholipids, and are stable when the level of PC, which acts as a surfactant, is sufficiently high (Krahmer et al., 2011). Below this concentration, an emulsion of small LDs (less than a micrometer in diameter) in aqueous buffer undergo spontaneous

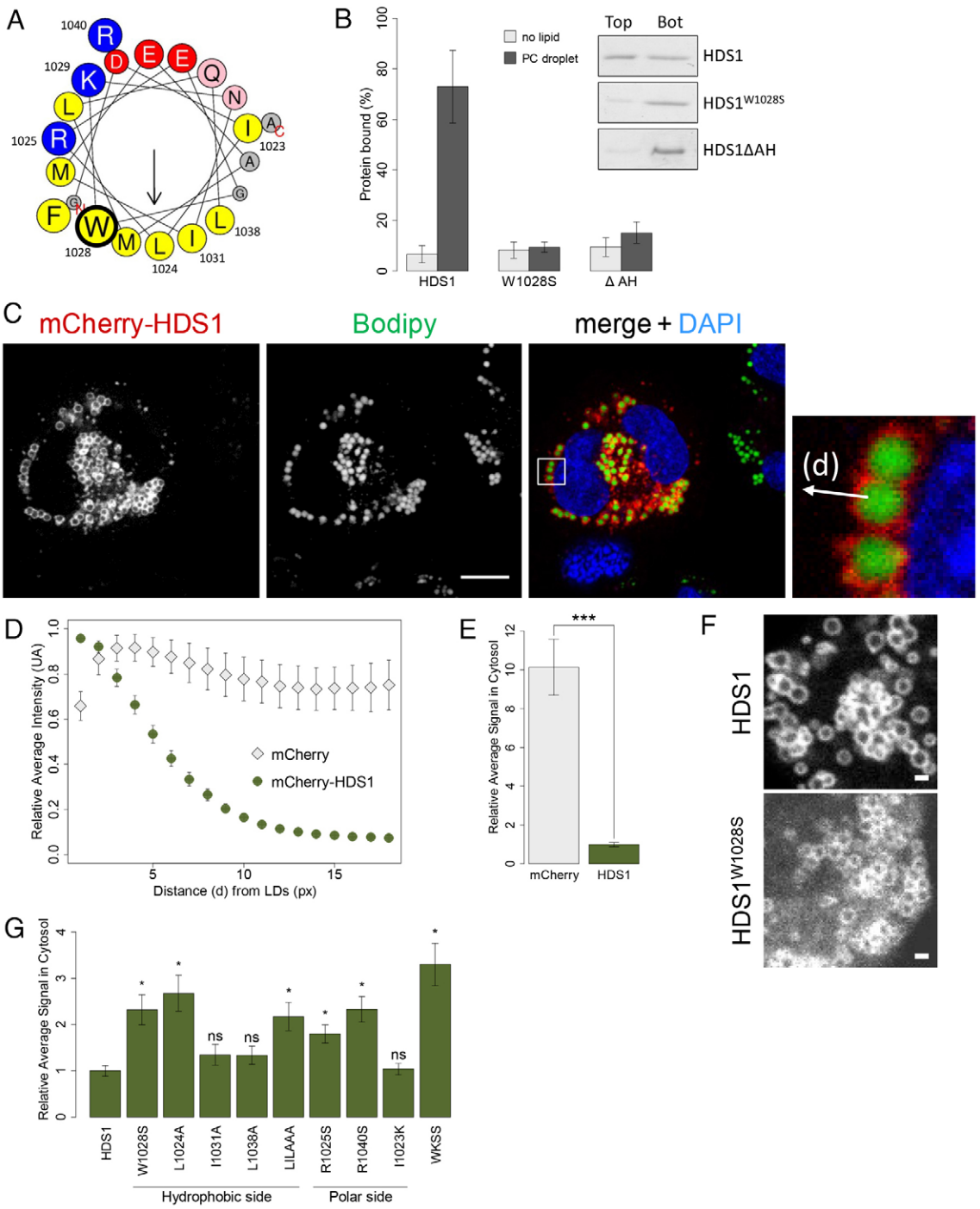

Fig. 3. An amphipathic region in HDS1 is required for HDS1 binding to LDs in cells and *in vitro*. (A) Helical wheel plot of a portion of the predicted C-terminal amphipathic helix (GBF1 1021–1041) (AH) of HDS1, showing the positions of mutated residues. α-helical properties were calculated using Heliquest software (heliquest.ipmc.cnrs.fr/). (B) GST−HDS1, GST−HDS1 W1028S or GST−HDS1 ΔAH were incubated with or without artificial PC droplets then sucrose gradient flotations were performed. Percentage protein bound was determined as described in Fig. 2. Values are means ± standard deviation of at least three independent experiments. (C) HeLa cells expressing mCherry−HDS1 were treated with oleic acid, then fixed and stained with BODIPY to visualize LDs. White arrow in the inset labeled '(d)' is an example of the vector along which quantifications shown in D were obtained. Scale bar: 10 µm. (D) The LD localization of HDS1 was quantified using Imaris and ImageJ, as described in Materials and Methods. The relative average fluorescence intensity, plotted as a function of distance (d, see part C) from a point near the LD edge, measured in pixels (px). (E) Bar graph representing the average fluorescence intensity at 18 pixels in plots such as those shown in D, normalized against that obtained for wild-type HDS1. Error bars represent the 95% confidence interval. $***P<10^{-10}$ (standard *t*-test). (F) Images of HeLa cells expressing mCherry−HDS1 or mCherry–HDS1W1028S treated as in C. Scale bars: 1 µm. (G) HeLa cells expressing mCherry−HDS1 (wild type or mutants) were treated with oleic acid before being fixed and stained for LD visualization as in C. Quantifications of the association with LDs were performed as described in E. $*P<10^{-3}$ (standard *t*-test). LILAAA stands for HDS1 L1024A, I1031A, L1038A and WKSS stands for HDS1 W1028S, K1029S.

fusion to produce very large droplets. We tested two phospholipid compositions, either PC alone or Golgi mix liposomes containing 50 mol % PC, above the minimum concentration to stably maintain artificial LDs. Droplets of a relatively uniform size were produced by extrusion. Binding of proteins to artificial LDs was assayed by flotation, and to validate the method we first used different forms of myristoylated Arf1 (myr-Arf1) as a control. Arf1 in its GDP-bound form (myr-Arf1–GDP) is primarily soluble, whereas its GTP-bound form (myr-Arf1–GTP) is tightly membrane bound when binding is assayed on liposomes of a wide range of compositions, including PC alone (Antonny et al., 1997). Proteomics studies have indicated that Arf1–GTP is present on LDs purified from cells induced to form LDs by oleate treatment (Bartz et al., 2007b). When assayed on either pure PC or Golgi mix artificial droplets, myr-Arf1–GDP failed to bind, whereas myr-Arf1–GTP bound as efficiently to these artificial LDs as to liposomes (Fig. 2D). We then tested binding of GST–HDS1, and found that it associated efficiently with artificial droplets, in contrast to GST alone, which was unable to bind (Fig. 2E). There was no significant difference in binding to pure PC or Golgi mix droplets. These results demonstrate that HDS1 is capable of binding to a phospholipid monolayer surface *in vitro*, and that this domain can bind efficiently to artificial LDs containing only neutral phospholipids.

A predicted amphipathic helix in the HDS1 C-terminal region is necessary and sufficient for HDS1 binding to LDs in cells and to artificial droplets *in vitro*

The C-terminal region of HDS1 is predicted to form an extended amphipathic helix (AH) with the characteristics of a lipid-binding AH (supplementary material Fig. S3A). Within this region is a particularly highly conserved tryptophan residue (Bui et al., 2009), on the hydrophobic side of the predicted helix, within a smaller 21-amino-acid region with the best potential to form an AH (Fig. 3A). To determine whether this region affects the lipid-binding properties of HDS1 *in vitro*, we introduced the W1028S mutation and deletion of the 21-amino-acid AH of HDS1 into GST–HDS1 (region shown in Fig. 3A, ΔAH) and purified the proteins from *E. coli*. The HDS1-W1028S mutant failed to bind liposomes, as describe above (Fig. 2C). Both the HDS1-W1028S and ΔAH mutations abolished binding of HDS1 to artificial droplets (Fig. 3B). Hence the C-terminal amphipathic region of HDS is essential for binding to artificial droplets *in vitro*.

To test the importance of the amphipathic C-terminal region (Fig. 3A) in binding of HDS1 to LDs in cells (Fig. 3C), we first developed an algorithm to quantify the level of an mCherry-tagged protein associated with BODIPY-labeled LDs in fluorescence images. Fluorescence intensity was determined along a vector from a point within the LD interior at a fixed distance from the edge (to allow quantification of LDs of different sizes), and extending perpendicularly towards the cytosol (Fig. 3C, inset). If the protein is bound to LDs, maximum fluorescence will be found in a narrow region encircling the LD, and the relative fluorescence will decrease with increasing distance from the LD. If the protein is cytosolic, this value will be relatively constant at all points from the LD circumference. Normalized fluorescence values, averaged for all LDs in a cell, were plotted as a function of distance from the LD starting point. Results for cells expressing mCherry–HDS1 or mCherry alone are plotted in Fig. 3D. To simplify comparison of different HDS1 mutants for their capacity to associate with LDs, levels of protein in the cytosol were quantified. Specifically, the values of each plot at the plateau reached at a distance of 18 pixels (corresponding to ~2 μm) from the starting point were determined, and normalized against the value obtained for wild-type HDS1. The results obtained for cytosolic mCherry alone compared with wild-type mCherry-HDS1 are shown in Fig. 3E.

To test the idea that the C-terminal amphipathic region of HDS1 forms an AH, we mutated residues that would alter its amphipathic properties, and assayed the localization of the mutant HDS1 domains fused to mCherry. Positions of the residues within this region that were mutated are shown in Fig. 3A. Mutations in hydrophobic residues in the predicted non-polar face of the HDS1 AH (W1028S, L1024A) led to decreased LD association and an increase in the cytosolic pool of the domain (Fig. 3F,G). Interestingly, the L1024A mutation in a leucine residue predicted to be at the center of the proposed amphipathic α-helix (Fig. 3A), had a severe effect on localization of HDS1, whereas mutation of the adjacent leucines to alanines had little effect (Fig. 3G). The triple mutation of three hydrophobic residues on the non-polar face (L1024A, I1031A, L1038A) had the same effect on localization as the single L1024A mutation (Fig. 3G). Mutations in the charged residues of the polar face (R1025 and R1040) of the HDS1 AH also resulted in loss of LD association (Fig. 3G). A double mutant of both the conserved Trp on the hydrophobic side and a Lys residue on the polar side (W1028S, K1029S) had the strongest effect on localization of HDS1 (Fig. 3G). However, mutation of the isoleucine predicted to be at the interfacial region of the AH to a lysine (I1023K) had no significant effect on localization (Fig. 3G). Deletion of a major portion of the predicted amphipathic helix (residues 1021–1041) also reduced LD targeting of HDS1 in cells (supplementary material Fig. S3B). These results support the conclusion that the amphipathic property of this predicted helical region plays a crucial role in LD binding in cells.

Our results have shown that, both *in vivo* and *in vitro*, the C-terminal amphipathic region of the GBF1 HDS1is required for its binding to LDs. To determine whether this region is sufficient on its own to target LDs, we expressed amino acids 1021–1048 fused to mCherry in cells treated with oleic acid. This predicted amphipathic helix was able, on its own, to localize to LDs (Fig. 4A). Compared with the full-length HDS1 domain, there was a higher level of the C-terminal AH in the cytosol (Fig. 4B), suggesting that it targets less efficiently or is less stably associated with LDs. *In vitro*, the C-terminal amphipathic helical region of HDS1 (amino acids 1005–1048 fused to GST) exhibited a high level of binding both to liposomes of different composition, and to artificial droplets (Fig. 4C). Hence the C-terminal AH of HDS1 is a lipid-binding motif, which can target both a monolayer droplet surface and a lipid bilayer, *in vitro* and in cells.

The catalytic Sec7 domain modulates the lipid-binding domain of HDS1

Our results have shown that the HDS1 domain expressed in oleic-acid-treated cells localizes very efficiently to LDs, with little if any localization to other organelles detectable at steady state. To further understand this localization mechanism, we determined how stably mCherry–HDS1 is associated with LDs by fluorescence recovery after photobleaching (FRAP) analysis. Little if any significant fluorescence recovery was detected up to

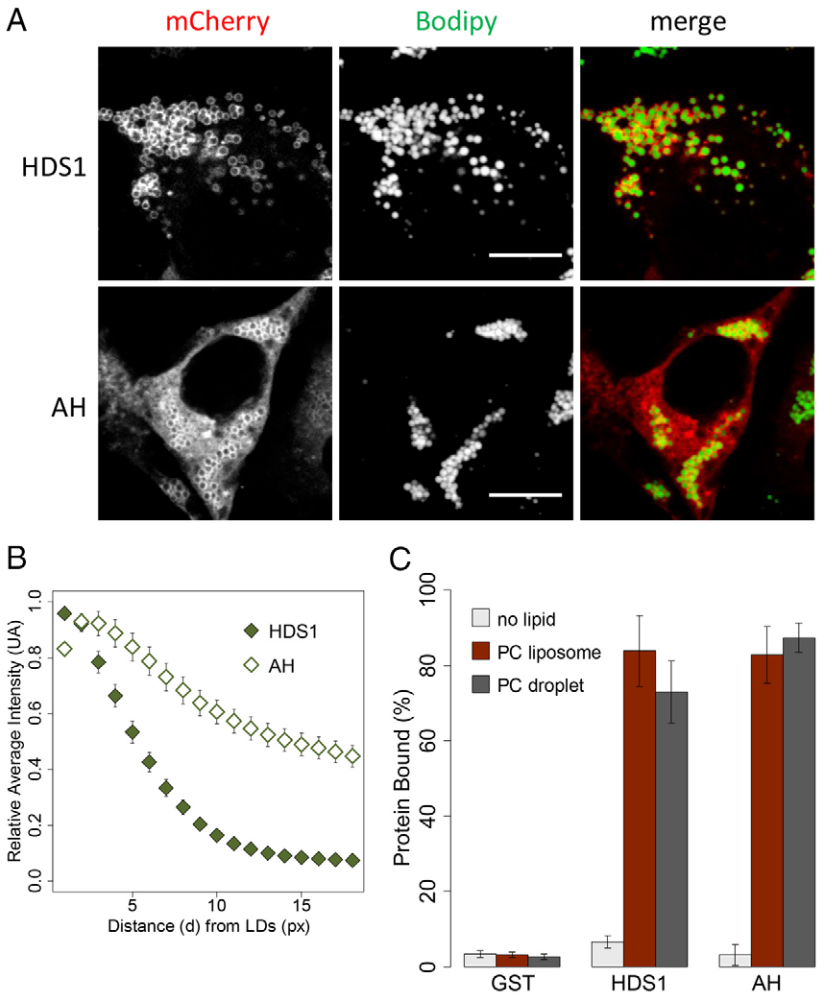

Fig. 4. A C-terminal amphipathic helix within HDS1 targets LDs in cells and artificial droplets *in vitro*. (A) HeLa cells expressing mCherry−HDS1 or mCherry−AH (GBF1 1021–1048) were treated with oleic acid then fixed and colocalization with LDs monitored by staining with BODIPY. Scale bars: 10 µm. (B) Localization of mCherry−HDS1 and mCherry−AH (GBF 11021–1048) quantified as in Fig. 3D. (C) GST, GST−HDS1 or GST−AH (GBF1 1005–1048) were incubated with either PC liposomes, artificial PC droplets or no lipid at 37°C for 30 minutes. For each protein, the percentage of total protein in the top fraction was determined as described in Fig. 2. Values are means ± standard deviation of at least three independent experiments.

6 minutes after photobleaching of an entire LD, indicating a slow replenishment of the majority of mCherry–HDS1 onto the LD surface (Fig. 5A, quantification shown in Fig. 5B). Hence LD-associated mCherry–HDS1 does not rapidly exchange with other pools within the cell. In cells not treated with oleic acid, HDS1 was found associated both with the few LDs present, and with structures in close proximity to the ER (Fig. 6A and data not shown). Subcellular fractionation indicated that the majority of HDS1 is present in the membrane fraction under these conditions (Fig. 6C). Hence HDS1 is targeted to membrane structures when not associated with LDs.

The fact that once associated with LDs, HDS1 is not readily exchanged, suggests that it might be important for cells to regulate this tight association. Indeed, in contrast to HDS1 alone, only a small fraction of full-length GBF1 is found at LDs in cells treated with oleic acid (Soni et al., 2009), suggesting regulation of its localization. To determine whether other domains of GBF1 are involved in membrane association, we expressed larger fragments of the protein. Strikingly, we found that the Sec7 domain–HDS1 tandem expressed in cells had a predominantly cytosolic localization, both by fluorescence imaging (Fig. 6A,B) and fractionation (Fig. 6C). In addition, the purified Sec7–HDS1 tandem was unable to associate with liposomes *in vitro*, in stark contrast to HDS1 alone (Fig. 6D,E). Hence the Sec7 domain modulates the lipid-binding capacity of HDS1, inhibiting its ability to bind membranes both *in vitro* and in cells. Because the N-terminal region of yeast Sec7p, including both the Sec7 and HDS1 domains, binds to membranes only in the presence of Arf1 (Richardson et al., 2012), we tested the idea that the presence of the Sec7 domain might now confer a requirement for Arf1 in liposome binding *in vitro*. The Sec7–HDS1 tandem was therefore incubated with liposomes in the presence of myr-Arf1. However, neither the GDP-bound nor the GTP-bound forms of myr-Arf1 increased the level of binding of Sec7–HDS1 to liposomes (Fig. 6E).

Given that the Sec7–HDS1 tandem does not localize to membranes in cells or to liposomes *in vitro*, we were interested in determining which additional domains of GBF1 are required for membrane targeting. The C-terminal regions of GBF1 downstream of HDS2, although they may play a role, are not required for localization to ERGIC–Golgi membranes in cells (supplementary material Fig. S2). Hence all or part of the N-terminal region, containing two homology domains called DCB and HUS, is likely to be important for Golgi localization. Indeed, we found that N-terminal truncations of GBF1 that lacked the DCB domain failed to localize to ERGIC or Golgi structures (supplementary material Fig. S2). We then expressed a construct extending from the HUS domain to the end of the HDS2 domain,

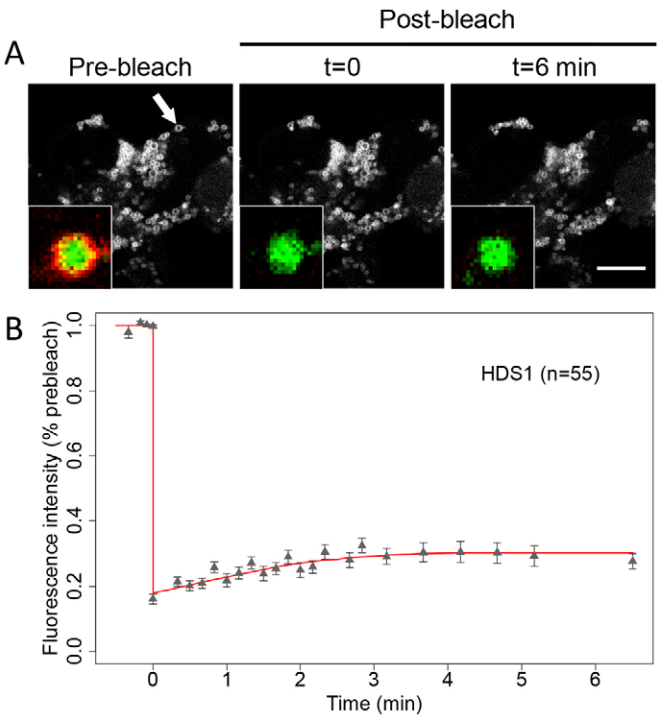

Fig. 5. The GBF1 HDS1 domain is stably associated with LDs. (A) HeLa cells expressing mCherry–HDS1 were treated with 400 µM oleic acid and incubated for 16–20 hours, then BODIPY was added prior to imaging. FRAP experiments were performed on isolated LDs as described in Materials and Methods. The arrow indicates an LD in which the mCherry signal was photobleached at time 0. Pre-bleach (left), immediately after bleach (middle), and post-bleach (right) images are shown. mCherry fluorescence is shown in the main panels; the insets are overlays of the channels showing the photobleached LD labeled with BODIPY. Scale bar: 10 µm. (B) Average fluorescence intensity in the red channel corrected for photobleaching is plotted as a function of time. 55 cells in three independent experiments performed as illustrated in A were analyzed. Error bars represent the 95% confidence interval.

encompassing both the catalytic Sec7 and HDS1 domains. This portion of GBF1 was associated with membranes in cells, as determined by fluorescence and fractionation analysis (Fig. 7A,B). However, this construct, like the N-terminal truncations, did not accumulate in the Golgi region, even when cells were treated with BFA (data not shown), although it did fractionate with membranes under these conditions (Fig. 7B). In cells treated with oleic acid, this HUS-to-HDS2 construct localized to LDs, similar to the HDS1 domain alone (Fig. 7A, bottom panels), although with a higher level in the cytosol (Fig. 7A, compare left and right bottom panels). Hence the HUS domain is not sufficient to mediate targeting of the downstream Sec7–HDS1–HDS2 domains to the Golgi, but requires in addition the DCB domain for Golgi localization.

Discussion

We demonstrate here that the peripherally associated regulator GBF1 localizes to lipid droplets (LDs) and to Golgi membranes through the same lipid-binding domain. GBF1, an activator of the Arf1 small G protein, is the first Arf1-GEF to function in the secretory pathway, and also plays an important role in LD metabolism (Donaldson and Jackson, 2011; Walther and Farese, 2012). Two domains of GBF1, HDS1 and HDS2, localize on their own to LDs in cells, whereas the full-length GBF1 protein localizes primarily to membranes of the secretory pathway, even in cells induced to produce LDs by treatment with fatty acids (Ellong et al., 2011; Soni et al., 2009). In this study, we focused on the HDS1 domain, located directly downstream of the catalytic Sec7 domain of GBF1, showing that it is capable of binding both bilayer liposomes and monolayer droplets *in vitro*. We also show that this potent LD-binding capacity of HDS1 is attenuated by the Sec7 domain, because the Sec7 domain–HDS1 tandem is soluble, both *in vitro* and in cells. Further addition of the upstream HUS domain results in a construct that can bind to membranes in cells, but does not accumulate on Golgi or ERGIC membranes at steady state. The full N-terminal region is required for GBF1 to maintain a persistent association with Golgi membranes.

During Golgi maturation, there is sequential activation of Arf1, first by a GBF family member at the *cis*-Golgi, then by a BIG family member at the *trans*-Golgi (Gillingham and Munro, 2007). Fromme and colleagues have proposed that the Arf1-dependent interaction of the Sec7p HDS1 domain is important to restrict binding of this late-acting Arf-GEF to membranes on which Arf1 has already been activated (Richardson et al., 2012). In this context, it is significant that the GBF1 HDS1 domain does not require Arf1 for binding, nor does activated Arf1 enhance binding of the HDS1 domain to liposomes *in vitro*. The Arf1-independent binding of GBF HDS1 and the Arf1-dependent lipid binding of the equivalent domain in BIG/Sec7 will ensure that GBF1 Arf-GEFs are recruited prior to BIG/Sec7 proteins, thus providing directionality in trafficking through the Golgi.

Together with these previous studies, our results support the idea of a general mechanism for binding of the GBF and BIG Arf-GEFs to membranes. For GBF1, both the HDS1 and HDS2 domains are required for GBF1 localization in cells, and the N-terminal region, which has been shown to bind to Rab1 (Monetta et al., 2007), is necessary to target GBF1 to Golgi membranes. Localization of BIG1, a mammalian and *Drosophila* homologue of yeast Sec7p, to late Golgi membranes requires binding of the BIG1 N-terminus to activated Arl1, a marker of the late Golgi (Christis and Munro, 2012). Hence, as for GBF1, both interaction of the HDS1 domain directly with lipids, and interaction of the N-terminus with another small G protein are involved in specific targeting of the BIG/Sec7 Arf-GEFs.

Our *in vitro* data indicate that HDS1, through its C-terminal amphipathic region, is able to efficiently bind to liposomes or artificial droplets containing PC alone. Hence a specific phosphorylated phosphoinositide, other charged lipids, or cholesterol are not required for lipid binding by HDS1, in keeping with the composition of both early Golgi membranes and LDs. Interestingly, a recent study has shown that a larger region of GBF1, including HDS1 and HDS2, as well as a 90-amino-acid region downstream, can target the leading edge of migrating neutrophils through specific recognition of phosphatidylinositol 3-phosphate and other products of phosphoinositide 3-kinase gamma (Mazaki et al., 2012). HDS1 and HDS2 on their own do not bind to phosphatidylinositol 3-phosphate, nor target the leading edge, but require the 90-amino-acid proline-rich region immediately downstream of HDS2 for this targeting. The fascinating picture that emerges is that the HDS1 domain (and probably HDS2 as well) are lipid-binding domains that have the capacity to bind to different membranes in cells, with other

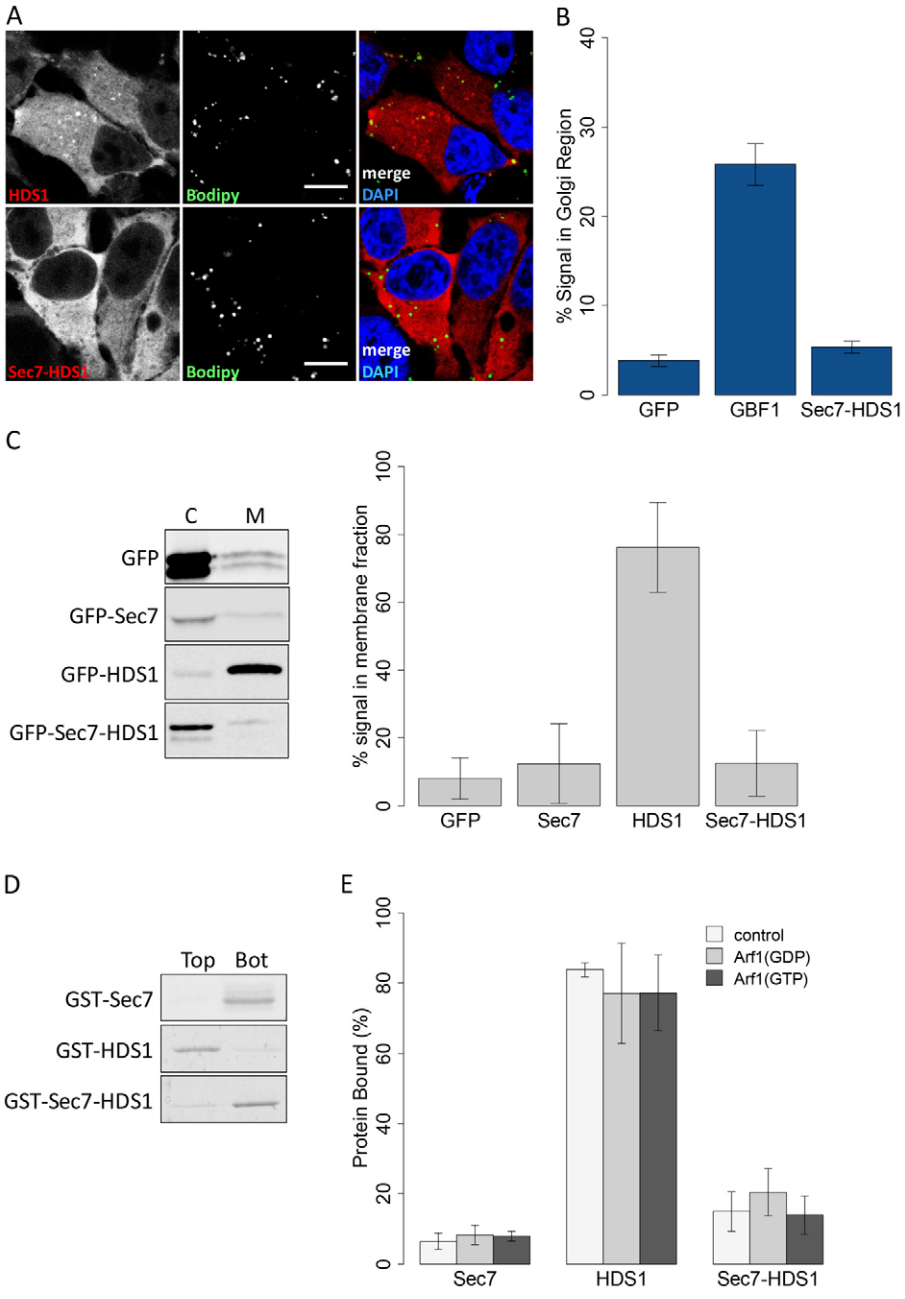

Fig. 6. The catalytic Sec7 domain of GBF1 inhibits membrane localization of HDS1, both in cells and *in vitro*. (A) HeLa cells expressing mCherry−HDS1 or the mCherry−Sec7−HDS1 tandem were fixed and stained to visualize LDs as described in Fig. 3. Scale bars: 10 µm. (B) HeLa cells expressing GFP, GFP−GBF1 or GFP−Sec7−HDS1 were incubated with 10 µg/ml BFA for 10 minutes at 37℃ then fixed and immunostained for Golgi localization, and the signal within the Golgi region was calculated as described in Materials and Methods. Error bars represent the 95% confidence interval. (C) Fractionation of HeLa cells (not treated with BFA) expressing GFP, GFP−Sec7, GFP−HDS1 or GFP−Sec7−HDS1 was performed as described in Fig. 1. Representative images of western blots are shown (left panel); the means and standard deviation of at least three experiments were calculated (right panel). C, cytosolic fraction; M, membrane fraction. (D) Flotation assay in which azolectin liposomes were incubated with either GST−HDS1, GST−Sec7 or GST−Sec7−HDS1. (E) Azolectin liposomes were loaded with Myr-Arf1(GDP), with Myr-Arf1(GTP), or not loaded with Myr-Arf1 (control), then incubated with either GST−HDS1, GST−Sec7 or GST−Sec7−HDS1. Percentage protein bound was determined as described in Fig. 2. Values are means ± standard deviation of at least three independent experiments.

regions of the GBF1 protein conferring specific information that targets the protein either to membranes of the early secretory pathway, LDs of oleic-acid-treated cells or the leading edge of migrating cells. For Golgi targeting of GBF1, protein–protein interactions are probably involved in addition to the protein–lipid interaction we reveal here. For LD localization of either GBF1 or the HDS1 domain alone, we have not ruled out the possibility that protein–protein interactions are involved in targeting. Although the HDS1 domain can localize to liposomes *in vitro* in the absence of additional proteins, we have evidence of interactions with LD-localized proteins that may possibly contribute to targeting (Ellong et al., 2011); coincidence detection mechanisms involving both may operate. Further studies are required to determine whether protein–lipid interactions may be solely responsible for targeting HDS1 to LDs, and by what mechanism.

The C-terminal region of the lipid-binding HDS1 domain of GBF1 is an amphipathic region predicted to form an α-helix on membranes. We have shown here that this region on its own is able to bind to LDs in cells, as well as to droplets *in vitro*, indicating that it is an LD targeting motif. Our mutagenesis analysis of this region supports the conclusion that it forms an amphipathic helix *in vitro* and in cells, and that this property is important for its targeting to LDs. Interestingly, other proteins, including perilipins (Bulankina et al., 2009), hepatitis C virus (HCV) core protein (Boulant et al., 2006), HCV NS5A protein, the antiviral peptide viperin (Hinson and Cresswell, 2009) and CTP:phosphocholine cytidylyltransferase α (CCTα) (Krahmer et al., 2011), all have amphipathic helices that are necessary and sufficient for targeting to LDs. Because the LD surface is a phospholipid monolayer, amphipathic helices are ideal

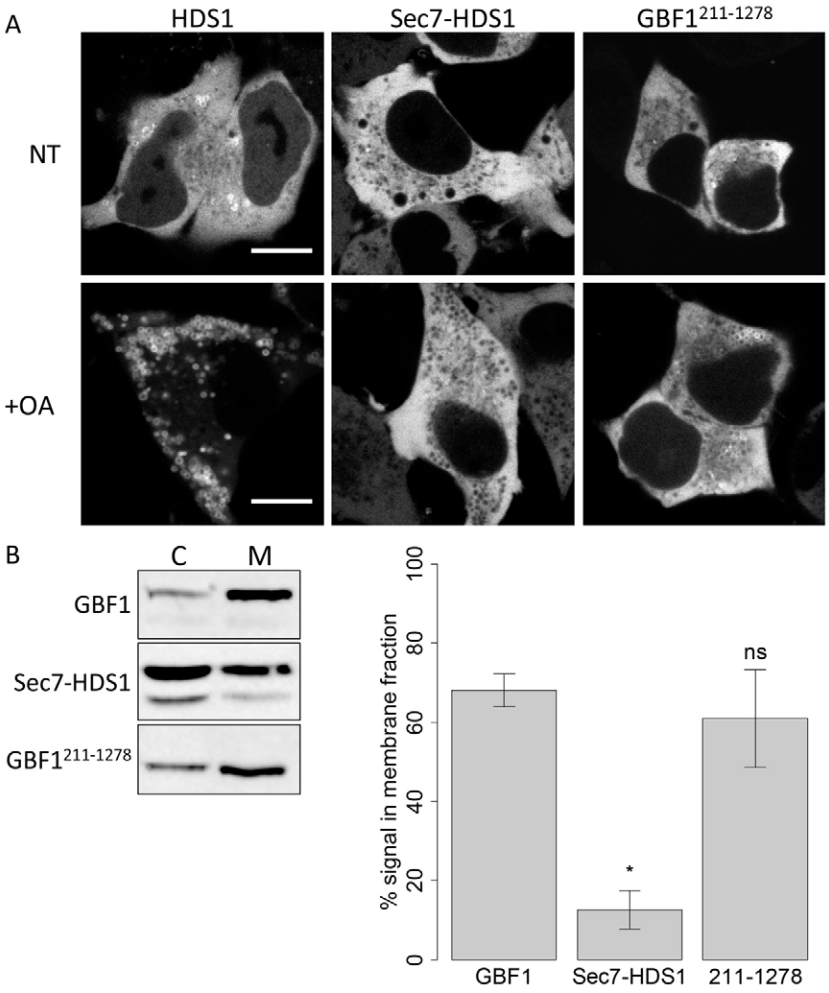

Fig. 7. The N-terminal region of GBF1 is required for maintenance of Golgi localization in cells. (A) HeLa cells expressing Venus−HDS1, GFP−Sec7−HDS1 or Venus−GBF1 211–1278 were treated (+OA) or not (NT) with 400 µM oleic acid, then imaged by confocal microscopy at 37℃. Scale bars: 10 µm. (B) HeLa cells expressing the indicated GBF1 construct were treated with BFA before processing for fractionation as described. The image shown is representative of at least two independent transfections. C, cytosolic fraction; M, membrane fraction. Quantification was performed as described in Fig. 1; means ± standard deviation from at least two independent experiments are shown.

localization devices, as they enter the interfacial region of only a single phospholipid monolayer. Although HDS1 can bind both to bilayer liposomes and droplets surrounded by a phospholipid monolayer *in vitro*, it localizes primarily to LDs in cells, in a stable manner. Other LD-associated proteins that are localized through AHs, including specific perilipins (Wang et al., 2009) and CCTα (Krahmer et al., 2011) are also stably associated with the LD surface. This could be due to either interactions of these AH-containing proteins with other LD resident proteins, or the biophysical properties of the LD phospholipid monolayer surface that lead to a stable association of an AH once it is bound. Interestingly, in addition to AH-containing LD proteins, the enzyme catalyzing the first step in triglyceride biosynthesis, glycerol-3-phosphate acyltransferase 4 (GPAT4), has been shown to localize both to the ER and to LDs, and once on the LD surface, it does not return to the ER (Wilfling et al., 2013). This property may be a general principle of LD-binding proteins.

Materials and Methods

Plasmids and antibodies

Plasmids used in this study are listed in supplementary material Table S1. All constructs were confirmed by DNA sequencing. HDS1 was cloned into pGEX-4T1 using *Eco*RI and *Sal*I sites; Sec7 and Sec7-HDS1 using *Bam*HI and *Xho*I sites. GBF1 and truncated forms were cloned into *Xho*I and *Kpn*I sites of pVenus-C1 and pmCherry-C1 (generous gifts from George Patterson, NIH, USA). GBF1-ΔHDS1, -ΔHDS2 and -ΔHDS1-2 were derived from pEGFP-GBF1-887Xho (which has a *Xho*I site after amino acid 887 of GBF1; a kind gift from Y. Mazaki and H. Sabe, Kumamoto, Japan) by PCR amplification of appropriate C-terminal regions of GBF1 and cloning into *Xho*I and *Not*I sites. The following antibodies were used: mouse anti-GST (Sigma-Aldrich, St Louis, MO, USA), mouse anti-GFP (Roche Diagnostics, Indianapolis, IN, USA), mouse anti-GBF1 (BD Biosciences, Franklin Lakes, NJ, USA), rabbit anti-ERGIC53/p58 (Sigma-Aldrich), mouse anti-β-actin (Abcam, Cambridge, MA, USA), rabbit anti-ATGL (Cell Signaling Technology, Danvers, MA, USA), guinea pig anti-ADRP (Progen Biotechnik, Heidelberg, Germany), mouse anti-GM130 (BD Biosciences).

Expression and purification of recombinant proteins in *E. coli*

GST was expressed and purified as described previously (Ellong et al., 2011). Myr-Arf1 was purified from BL21Gold(DE3) cells transformed with pET11d-Arf1 and pBB(NMT) (generous gifts of Bruno Antonny, Sophia Antipolis, France) as described (Franco et al., 1995). GST-HDS1 (wild type, W1028S and ΔAH) were induced in *E. coli* strain C41(DE3) with isopropyl-β-D thiogalactopyranoside (IPTG, Euromedex, Strasbourg, France) at 30℃ for 4 hours. GST-Sec7-GBF1 and GST-Sec7-HDS1-GBF1 were induced in *E. coli* strain Rosetta(DE3)pLys with IPTG at 20℃ overnight (for GST-Sec7) or at 37℃ for 2 hours (for GST-Sec7-HDS1). For HDS1-containing proteins, lysis was carried out in TEX buffer (50 mM Tris-HCl pH 8.0, 100 mM NaCl, 1 mM EDTA, 1 mM DTT) in the presence of Complete Mini Protease Inhibitor cocktail (Roche Diagnostics), 2 mM phenylmethylsulfonyl fluoride (PMSF, USB), 0.5% Nonidet P40 substitute (NP40, Sigma-Aldrich) and 0.5% Triton X-100 (Sigma-Aldrich). Proteins were purified on a glutathione–Sepharose 4B resin (GE Healthcare, Little Chalfont, Buckinghamshire, UK) at 4℃ and eluted in 15 ml TEX supplemented with 50 mM reduced L-glutathione, 0.5% NP40 and 0.5% Triton X-100, then dialyzed against 10 mM Tris-HCl pH 8.0, 50 mM NaCl, 1 mM DTT buffer and concentrated with a Vivaspin system (Sartorus Stedim, Palaiseau, France). Concentrations were determined with BCA Protein Assay kit (Thermo Scientifique/Pierce Brebières, France).

For GST–Sec7–GBF1, cells from a 1 liter culture were sonicated in 20 ml of buffer A (100 mM sodium phosphate pH 8.0, 300 mM NaCl, 2 mM DTT) supplemented with 0.5% sodium deoxycholate and Complete Mini Protease Inhibitor cocktail. Cells were centrifuged and the supernatant was loaded on a glutathione–Sepharose 4B column. The resin was washed with buffer A, then with buffer A containing increasing concentration of reduced L-glutathione: 10 mM, 30 mM then 50 mM. Protein eluted in the final two washing steps was dialyzed against 10 mM Tris-HCl pH 8.0, 100 mM NaCl, 2 mM DTT buffer, and concentrated with a Vivaspin system.

Liposome and artificial droplet preparation

Azolectin (L-phosphatidylcholine type IV-S) was from Sigma-Aldrich; other lipids were from Avanti Polar Lipids/Coger (Paris, France). Golgi-mix phospholipids contained (mol%) egg PC (50), egg PE (19), brain PS (5), liver PI (10), cholesterol (16), NBD-PE (0.2). For liposome preparation, a dried film was prepared in a glass tube by evaporation of a mixture of the indicated lipids in chloroform (azolectin, Golgi mix or PC only) and resuspended in HK buffer (50 mM HEPES-KOH pH 7.2 and 120 mM potassium acetate). After five freeze–thaw cycles, the liposome suspension was extruded 19 times through polycarbonate filters (pore size of 0.4 µm for defined composition liposomes or 0.1 µm for azolectin liposomes) using a hand extruder (Avanti Polar Lipids) at a final lipid concentration of 20 mg/ml for azolectin liposomes and 1 mM for defined composition liposomes. Liposomes were stored at room temperature and used within 2 days after preparation. Artificial droplets were prepared as described previously (Thiam et al., 2013). Briefly, 70 µl triolein (Sigma-Aldrich) were mixed in a glass tube with 0.5 µmol phospholipids and 1 pmol NBD-PE. Chloroform was evaporated under an argon flow, then under vacuum. The oil was dispersed in 1 ml of HK buffer by vigorous vortexing, then extruded nine times through a 1 µm pore size nitrocellulose membrane. Artificial droplets were stored at room temperature and used the day of the preparation.

Lipid binding assays

For proteins purified in the presence of detergent, Pierce Detergent Removal Spin Columns (Thermo Scientifique/Pierce) were used according to manufacturer's instructions. Proteins were incubated with liposomes or artificial droplets in HK buffer containing 1 mM $MgCl_2$ and 1 mM DTT (HKM buffer) at 37℃ for 30 minutes in a total volume of 58 µl. Nucleotide (100 µM of GTP or GDP) was loaded onto Myr-Arf1 in the presence of lipids (liposomes or droplets) and 2 mM EDTA for 30 minutes at 37℃, then 2 mM $MgCl_2$ was added. The suspension was adjusted to 31.5% sucrose by adding 42 µl of a 75% w/v sucrose solution in HKM buffer, then overlaid with 75 µl HKM buffer containing 25% w/v sucrose, and finally 10 µl HKM buffer. The sample was centrifuged at 55,000 rpm (259,000 ***g***) in a Beckman rotor TLS 55 for 1 hour at 20℃. The bottom (95 µl), middle (75 µl) and top (20 µl) fractions were manually collected from the bottom using a syringe (Hamilton Company, Bonaduz, Switzerland) and analyzed by SDS–PAGE using Blue Silver Staining (Candiano et al., 2004). Gels were scanned and quantifications performed using ImageJ (NIH, Bethesda, MD, USA). Except for azolectin liposomes, the recovery of the liposomes/artificial droplets after fraction collection was checked using NBD-PE fluorescence with a FUJI LAS-3000 fluorescence imaging system.

Cell culture and transfection

HeLa and Cos7 cells were grown in Dulbecco's modified Eagle's medium (DMEM) supplemented with 4.5 g/l glucose, 4 mM L-glutamine, 1 mM sodium pyruvate (GE Healthcare) and 10% fetal bovine serum (Invitrogen, Carlsbad, CA, USA). Retinal pigment epithelial (RPE-1) cells were grown in DMEM/Ham's F12 medium (1:1; PAA, Les Mureaux, France) supplemented with 10% FBS. Subconfluent cells were transfected with plasmids using Lipofectamine 2000 (Invitrogen) or FuGENE-6 (Roche Diagnostics). Oleic acid (OA) complexed with BSA was prepared as described previously (Soni et al., 2009). For overnight OA treatment, at 8 hour post-transfection cells were treated with 100–400 µM OA and incubated for an additional 16–20 hours before preparation for imaging. BFA (Sigma-Aldrich) was added to cells at 5–10 µg/ml for 5–10 minutes before preparation for imaging.

Immunofluorescence and microscopy

For immunofluorescence microscopy, HeLa cells were grown on glass coverslips and fixed with 4% formaldehyde (Sigma-Aldrich) at room temperature for 15 minutes. Cells were incubated for 40 minutes to 1 hour in blocking buffer [20 mM glycine, 0.3% BSA, 0.01% saponin (Sigma-Aldrich, St Louis, MO, USA) in PBS buffer] at room temperature, and probed with primary antibody for 16 hours at 4℃, then with secondary antibody for 1 hour at room temperature. To stain the LD cores, cells were incubated with 1 µg/ml BODIPY 493/503 (Invitrogen) in PBS for 20 minutes at room temperature. Coverslips were mounted on glass slides using Prolong Antifade Gold (Invitrogen), sealed and stored at 4℃. Images and z-stack images were acquired using an inverted confocal laser scanning microscope (TCS SP5 AOBS Tandem resonant Scanner, Leica). The percentage of signal in the Golgi region was determined with the following equation:

$$I_{Golgi}(\%) = \frac{Int_{Golgi} - (Avg_{background} A_{Golgi})}{Int_{All} - (Avg_{background} A_{all})}, \quad (1)$$

where Int_{Golgi} is the intensity of the signal within the Golgi region automatically segmented with the GM130 signal, $Avg_{background}$ is the average noise measured in a region outside cell, A_{Golgi} is the area of the Golgi region, Int_{all} is the intensity of the whole image and A_{all} is the area of the image.

Fluorescence recovery after photobleaching (FRAP) experiments were performed as described previously (Soni et al., 2009). Three pre-bleach images were taken at low laser intensity. Then, the region of interest (ROI) corresponding to one single isolated LD was scanned three times with the appropriate laser line at full laser power to photobleach mCherry fluorescence. Fluorescence recovery into the ROI was monitored immediately after the bleach by time-lapse imaging at low-intensity illumination. The values were plotted using the following equation:

$$I_{cell}(t) = \left(\frac{I_{ROI}(t)}{I_{ROI}(t_0)}\right)\left(\frac{I_{cell}(t)}{I_{cell}(t_0)}\right)100, \quad (2)$$

where $I_{cell}(t_0)$ is the prebleach whole cell intensity, $I_{cell}(t)$ is the whole cell intensity at time t, $I_{ROI}(t_0)$ is the intensity in the bleached ROI before the bleach, and $I_{ROI}(t)$ is the intensity in the bleached ROI at time t. For each quantification, the number of cells imaged, from at least three independent transfections, is indicated (n).

Quantification of protein distribution around LDs

Image processing algorithms were developed to quantify the intensity of the signal as a function of the distance to LD volume using Imaris 7.6 (Bitplane) and ImageJ. All images were processed with the same parameters. LD size and position were determined first with the Imaris Spots detection tool using the region growing option on the green channel which correspond to the LD core stained with BODIPY 493/503. An image of isolated LD positions was then generated and exported to ImageJ in order to identify pixels which were inside the cell and outside LDs in the red channel (pmCherry fusion proteins). These pixels were obtained using filtering and mathematical morphology in the following way: an exact Euclidean distance transformation in 3D was first performed from the image of isolated LD positions to create a new image where the values of the intensities of pixels were equal to the distance from the center of LD previously obtained. Successive thresholds of this distance map were performed in order to create a mask for each distance from LDs. These masks were used to select pixels and were quantified in the red channel. Another mask corresponding to borders of the cell was obtained by filtering (median filter) and thresholding with a low level in the red channel. Finally, the average signal in the red channel of the pixels included in the mask of the cell was calculated for each distance to the center of LDs. The average signal was normalized against the maximum value and plotted against the distance to LDs to generate an intensity profile of the red channel signal along the cross section of LDs.

Subcellular fractionation

Cells were incubated with 10 µg/ml BFA for 10 minutes at 37℃, then washed with ice-cold PBS, scraped from plates and centrifuged at 1500 ***g*** for 5 minutes at 4℃. Approximately 1.5×10^6 cells were used for each condition. Cell pellets were resuspended in 200 µl of 50 mM HEPES-KOH pH 7.5, 100 mM KCl, 1 mM $MgCl_2$, 1 mM DTT, supplemented with protease inhibitors (GE Healthcare), by five passages through a 26-gauge needle on ice and disrupted by five passages through a 30-gauge needle on ice. Cell lysates were centrifuged at 5000 ***g*** for 10 minutes at 4℃, and 100 µl of the post-nuclear supernatant were centrifuged at 100,000 ***g*** for 50 minutes at 4℃ using a Beckman swing rotor (TLS-55). Two fractions, cytosol (supernatant) and membranes (pellet), were collected. The membrane fraction was resuspended in 50 µl homogenization buffer supplemented with 1% Triton X-100, 1% NP40 and 0.1% SDS (Invitrogen). Equivalent volumes of the two fractions were then analyzed by SDS-PAGE, transferred to nitrocellulose membranes and blotted with an antibody against GFP. Images were acquired using a FUJI LAS-3000 fluorescence imaging system and quantification of at least three independent experiments was performed using ImageJ. The percentage of membrane-bound protein was calculated with the following equation:

$$\%_{membrane} = \frac{Den_{[M]}}{Den_{[M]} + 2(Den_{[C]})}, \quad (3)$$

where $Den_{[M]}$ is the density of the membrane fraction band and $Den_{[C]}$ is the density of the cytosolic fraction band.

Acknowledgements

We thank Ting Niu, George Patterson, Yuichi Mazaki, Hisataka Sabe and Bruno Antonny for plasmids. We are grateful to Bruno Antonny

for communication of the artificial droplet assay, and to Ting Niu for preliminary GBF1 localization results.

Author contributions

C.L.J. and S.B. conceived the project and designed experiments. S.B. and M.P.G. designed and performed experiments. V.C. developed the LD protein association algorithm. C.L.J. and S.B. wrote the manuscript.

Funding

This work was funded by grants from the Agence Nationale de la Recherche [grant number ANR2010-BLAN-1229-01 to C.L.J.]; the Fondation pour la Recherche Médicale [grant number INE20071110975 to C.L.J.]; the Centre National de la Recherche Scientifique, France and the Ministère de l'Enseignement Supérieur et de la Recherche [grant number 2010/7 to S.B.].

Supplementary material available online at
http://jcs.biologists.org/lookup/suppl/doi:10.1242/jcs.134254/-/DC1

References

Antonny, B., Beraud-Dufour, S., Chardin, P. and Chabre, M. (1997). N-terminal hydrophobic residues of the G-protein ADP-ribosylation factor-1 insert into membrane phospholipids upon GDP to GTP exchange. *Biochemistry* **36**, 4675-4684.

Bartz, R., Li, W. H., Venables, B., Zehmer, J. K., Roth, M. R., Welti, R., Anderson, R. G., Liu, P. and Chapman, K. D. (2007a). Lipidomics reveals that adiposomes store ether lipids and mediate phospholipid traffic. *J. Lipid Res.* **48**, 837-847.

Bartz, R., Zehmer, J. K., Zhu, M., Chen, Y., Serrero, G., Zhao, Y. and Liu, P. (2007b). Dynamic activity of lipid droplets: protein phosphorylation and GTP-mediated protein translocation. *J. Proteome Res.* **6**, 3256-3265.

Beck, R., Rawet, M., Wieland, F. T. and Cassel, D. (2009). The COPI system: molecular mechanisms and function. *FEBS Lett.* **583**, 2701-2709.

Behnia, R. and Munro, S. (2005). Organelle identity and the signposts for membrane traffic. *Nature* **438**, 597-604.

Beller, M., Sztalryd, C., Southall, N., Bell, M., Jäckle, H., Auld, D. S. and Oliver, B. (2008). COPI complex is a regulator of lipid homeostasis. *PLoS Biol.* **6**, e292.

Bigay, J. and Antonny, B. (2012). Curvature, lipid packing, and electrostatics of membrane organelles: defining cellular territories in determining specificity. *Dev. Cell* **23**, 886-895.

Bigay, J., Casella, J. F., Drin, G., Mesmin, B. and Antonny, B. (2005). ArfGAP1 responds to membrane curvature through the folding of a lipid packing sensor motif. *EMBO J.* **24**, 2244-2253.

Bonifacino, J. S. and Lippincott-Schwartz, J. (2003). Coat proteins: shaping membrane transport. *Nat. Rev. Mol. Cell Biol.* **4**, 409-414.

Boulant, S., Montserret, R., Hope, R. G., Ratinier, M., Targett-Adams, P., Lavergne, J. P., Penin, F. and McLauchlan, J. (2006). Structural determinants that target the hepatitis C virus core protein to lipid droplets. *J. Biol. Chem.* **281**, 22236-22247.

Bozza, P. T. and Viola, J. P. (2010). Lipid droplets in inflammation and cancer. *Prostaglandins Leukot. Essent. Fatty Acids* **82**, 243-250.

Bui, Q. T., Golinelli-Cohen, M. P. and Jackson, C. L. (2009). Large Arf1 guanine nucleotide exchange factors: evolution, domain structure, and roles in membrane trafficking and human disease. *Mol. Genet. Genomics* **282**, 329-350.

Bulankina, A. V., Deggerich, A., Wenzel, D., Mutenda, K., Wittmann, J. G., Rudolph, M. G., Burger, K. N. and Höning, S. (2009). TIP47 functions in the biogenesis of lipid droplets. *J. Cell Biol.* **185**, 641-655.

Candiano, G., Bruschi, M., Musante, L., Santucci, L., Ghiggeri, G. M., Carnemolla, B., Orecchia, P., Zardi, L. and Righetti, P. G. (2004). Blue silver: a very sensitive colloidal Coomassie G-250 staining for proteome analysis. *Electrophoresis* **25**, 1327-1333.

Christis, C. and Munro, S. (2012). The small G protein Arl1 directs the trans-Golgi-specific targeting of the Arf1 exchange factors BIG1 and BIG2. *J. Cell Biol.* **196**, 327-335.

Cohen, J. C., Horton, J. D. and Hobbs, H. H. (2011). Human fatty liver disease: old questions and new insights. *Science* **332**, 1519-1523.

Donaldson, J. G. and Jackson, C. L. (2011). ARF family G proteins and their regulators: roles in membrane transport, development and disease. *Nat. Rev. Mol. Cell Biol.* **12**, 362-375.

Ellong, E. N., Soni, K. G., Bui, Q. T., Sougrat, R., Golinelli-Cohen, M. P. and Jackson, C. L. (2011). Interaction between the triglyceride lipase ATGL and the Arf1 activator GBF1. *PLoS ONE* **6**, e21889.

Franco, M., Chardin, P., Chabre, M. and Paris, S. (1995). Myristoylation of ADP-ribosylation factor 1 facilitates nucleotide exchange at physiological Mg2+ levels. *J. Biol. Chem.* **270**, 1337-1341.

García-Mata, R., Szul, T., Alvarez, C. and Sztul, E. (2003). ADP-ribosylation factor/COPI-dependent events at the endoplasmic reticulum-Golgi interface are regulated by the guanine nucleotide exchange factor GBF1. *Mol. Biol. Cell* **14**, 2250-2261.

Gaspar, M. L., Jesch, S. A., Viswanatha, R., Antosh, A. L., Brown, W. J., Kohlwein, S. D. and Henry, S. A. (2008). A block in endoplasmic reticulum-to-Golgi trafficking inhibits phospholipid synthesis and induces neutral lipid accumulation. *J. Biol. Chem.* **283**, 25735-25751.

Gaspar, M. L., Hofbauer, H. F., Kohlwein, S. D. and Henry, S. A. (2011). Coordination of storage lipid synthesis and membrane biogenesis: evidence for cross-talk between triacylglycerol metabolism and phosphatidylinositol synthesis. *J. Biol. Chem.* **286**, 1696-1708.

Gillingham, A. K. and Munro, S. (2007). The small G proteins of the Arf family and their regulators. *Annu. Rev. Cell Dev. Biol.* **23**, 579-611.

Greenberg, A. S., Coleman, R. A., Kraemer, F. B., McManaman, J. L., Obin, M. S., Puri, V., Yan, Q. W., Miyoshi, H. and Mashek, D. G. (2011). The role of lipid droplets in metabolic disease in rodents and humans. *J. Clin. Invest.* **121**, 2102-2110.

Guo, Y., Walther, T. C., Rao, M., Stuurman, N., Goshima, G., Terayama, K., Wong, J. S., Vale, R. D., Walter, P. and Farese, R. V. (2008). Functional genomic screen reveals genes involved in lipid-droplet formation and utilization. *Nature* **453**, 657-661.

Hinson, E. R. and Cresswell, P. (2009). The antiviral protein, viperin, localizes to lipid droplets via its N-terminal amphipathic alpha-helix. *Proc. Natl. Acad. Sci. USA* **106**, 20452-20457.

Krahmer, N., Guo, Y., Wilfling, F., Hilger, M., Lingrell, S., Heger, K., Newman, H. W., Schmidt-Supprian, M., Vance, D. E., Mann, M. et al. (2011). Phosphatidylcholine synthesis for lipid droplet expansion is mediated by localized activation of CTP:phosphocholine cytidylyltransferase. *Cell Metab.* **14**, 504-515.

Liu, P., Ying, Y., Zhao, Y., Mundy, D. I., Zhu, M. and Anderson, R. G. (2004). Chinese hamster ovary K2 cell lipid droplets appear to be metabolic organelles involved in membrane traffic. *J. Biol. Chem.* **279**, 3787-3792.

Mazaki, Y., Nishimura, Y. and Sabe, H. (2012). GBF1 bears a novel phosphatidylinositol-phosphate binding module, BP3K, to link PI3Kγ activity with Arf1 activation involved in GPCR-mediated neutrophil chemotaxis and superoxide production. *Mol. Biol. Cell* **23**, 2457-2467.

Monetta, P., Slavin, I., Romero, N. and Alvarez, C. (2007). Rab1b interacts with GBF1 and modulates both ARF1 dynamics and COPI association. *Mol. Biol. Cell* **18**, 2400-2410.

Niu, T. K., Pfeifer, A. C., Lippincott-Schwartz, J. and Jackson, C. L. (2005). Dynamics of GBF1, a Brefeldin A-sensitive Arf1 exchange factor at the Golgi. *Mol. Biol. Cell* **16**, 1213-1222.

Panic, B., Whyte, J. R. and Munro, S. (2003). The ARF-like GTPases Arl1p and Arl3p act in a pathway that interacts with vesicle-tethering factors at the Golgi apparatus. *Curr. Biol.* **13**, 405-410.

Richardson, B. C., McDonold, C. M. and Fromme, J. C. (2012). The Sec7 Arf-GEF is recruited to the trans-Golgi network by positive feedback. *Dev. Cell* **22**, 799-810.

Saka, H. A. and Valdivia, R. (2012). Emerging roles for lipid droplets in immunity and host-pathogen interactions. *Annu. Rev. Cell Dev. Biol.* **28**, 411-437.

Soni, K. G., Mardones, G. A., Sougrat, R., Smirnova, E., Jackson, C. L. and Bonifacino, J. S. (2009). Coatomer-dependent protein delivery to lipid droplets. *J. Cell Sci.* **122**, 1834-1841.

Stehr, M., Elamin, A. A. and Singh, M. (2012). Cytosolic lipid inclusions formed during infection by viral and bacterial pathogens. *Microbes Infect.* **14**, 1227-1237.

Szul, T., Garcia-Mata, R., Brandon, E., Shestopal, S., Alvarez, C. and Sztul, E. (2005). Dissection of membrane dynamics of the ARF-guanine nucleotide exchange factor GBF1. *Traffic* **6**, 374-385.

Thiam, A.-R., Antonny, B., Wang, J., Delacotte, J., Wilfling, F., Walther, T. C., Beck, R., Rothman, J. E. and Pincet, F. (2013). COPI buds 60-nm lipid droplets from reconstituted water-phospholipid-triacylglyceride interfaces, suggesting a tension clamp function. *Proc. Natl. Acad. Sci. USA* [Epub ahead of pring].

Vamparys, L., Gautier, R., Vanni, S., Bennett, W. F., Tieleman, D. P., Antonny, B., Etchebest, C. and Fuchs, P. F. (2013). Conical lipids in flat bilayers induce packing defects similar to that induced by positive curvature. *Biophys. J.* **104**, 585-593.

Vanni, S., Vamparys, L., Gautier, R., Drin, G., Etchebest, C., Fuchs, P. F. and Antonny, B. (2013). Amphipathic lipid packing sensor motifs: probing bilayer defects with hydrophobic residues. *Biophys. J.* **104**, 575-584.

Walther, T. C. and Farese, R. V., Jr (2012). Lipid droplets and cellular lipid metabolism. *Annu. Rev. Biochem.* **81**, 687-714.

Wang, H., Hu, L., Dalen, K., Dorward, H., Marcinkiewicz, A., Russell, D., Gong, D., Londos, C., Yamaguchi, T., Holm, C. et al. (2009). Activation of hormone-sensitive lipase requires two steps, protein phosphorylation and binding to the PAT-1 domain of lipid droplet coat proteins. *J. Biol. Chem.* **284**, 32116-32125.

Wilfling, F., Wang, H., Haas, J. T., Krahmer, N., Gould, T. J., Uchida, A., Cheng, J. X., Graham, M., Christiano, R., Fröhlich, F. et al. (2013). Triacylglycerol synthesis enzymes mediate lipid droplet growth by relocalizing from the ER to lipid droplets. *Dev. Cell* **24**, 384-399.

Zechner, R., Zimmermann, R., Eichmann, T. O., Kohlwein, S. D., Haemmerle, G., Lass, A. and Madeo, F. (2012). FAT SIGNALS—lipases and lipolysis in lipid metabolism and signaling. *Cell Metab.* **15**, 279-291.

Zhao, X., Claude, A., Chun, J., Shields, D. J., Presley, J. F. and Melançon, P. (2006). GBF1, a cis-Golgi and VTCs-localized ARF-GEF, is implicated in ER-to-Golgi protein traffic. *J. Cell Sci.* **119**, 3743-3753.

SUPPLEMENTARY MATERIAL for

Targeting of the Arf-GEF GBF1 to lipid droplets and Golgi membranes

by Samuel Bouvet, Marie-Pierre Golinelli-Cohen, Vincent Contremoulins, and Catherine L. Jackson

Files in this Data Supplement:

* Supplementary Figures S1, S2, S3

* Supplementary Table S1

Figure S1

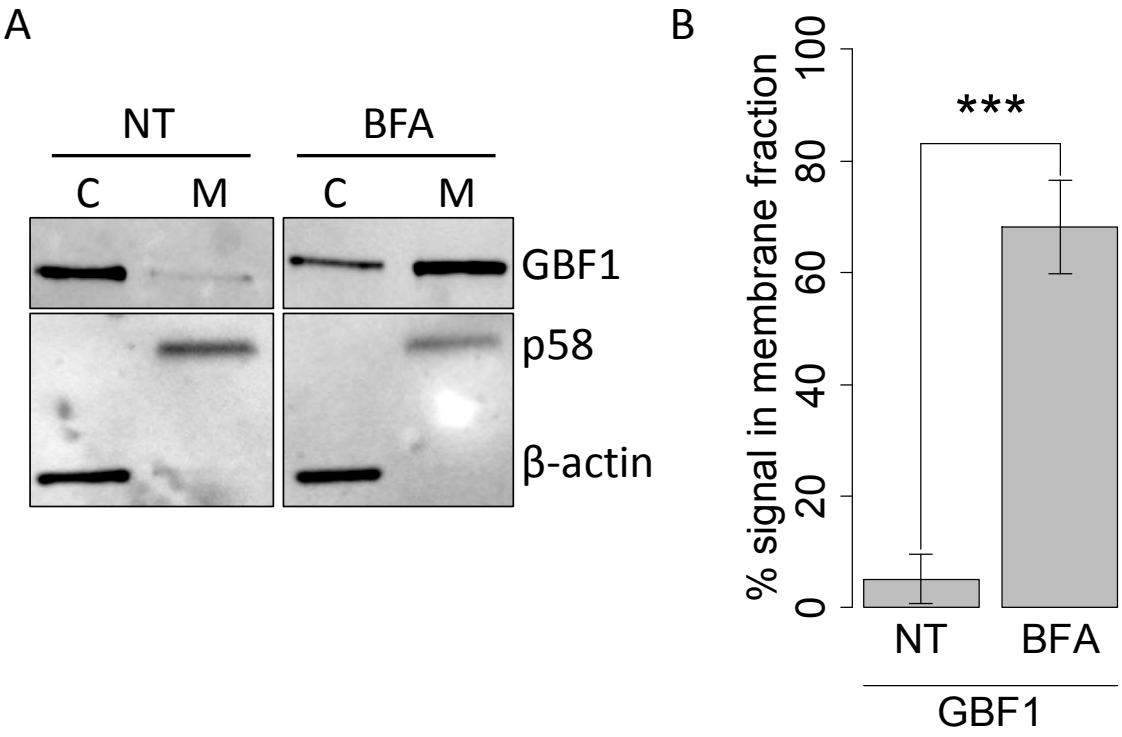
A
NT
BFA
C
M
C
M
GBF1
p58
β-actin
B
% signal in membrane fraction
0
20
40
60
80
100
***
NT
BFA
GBF1

Figure S2

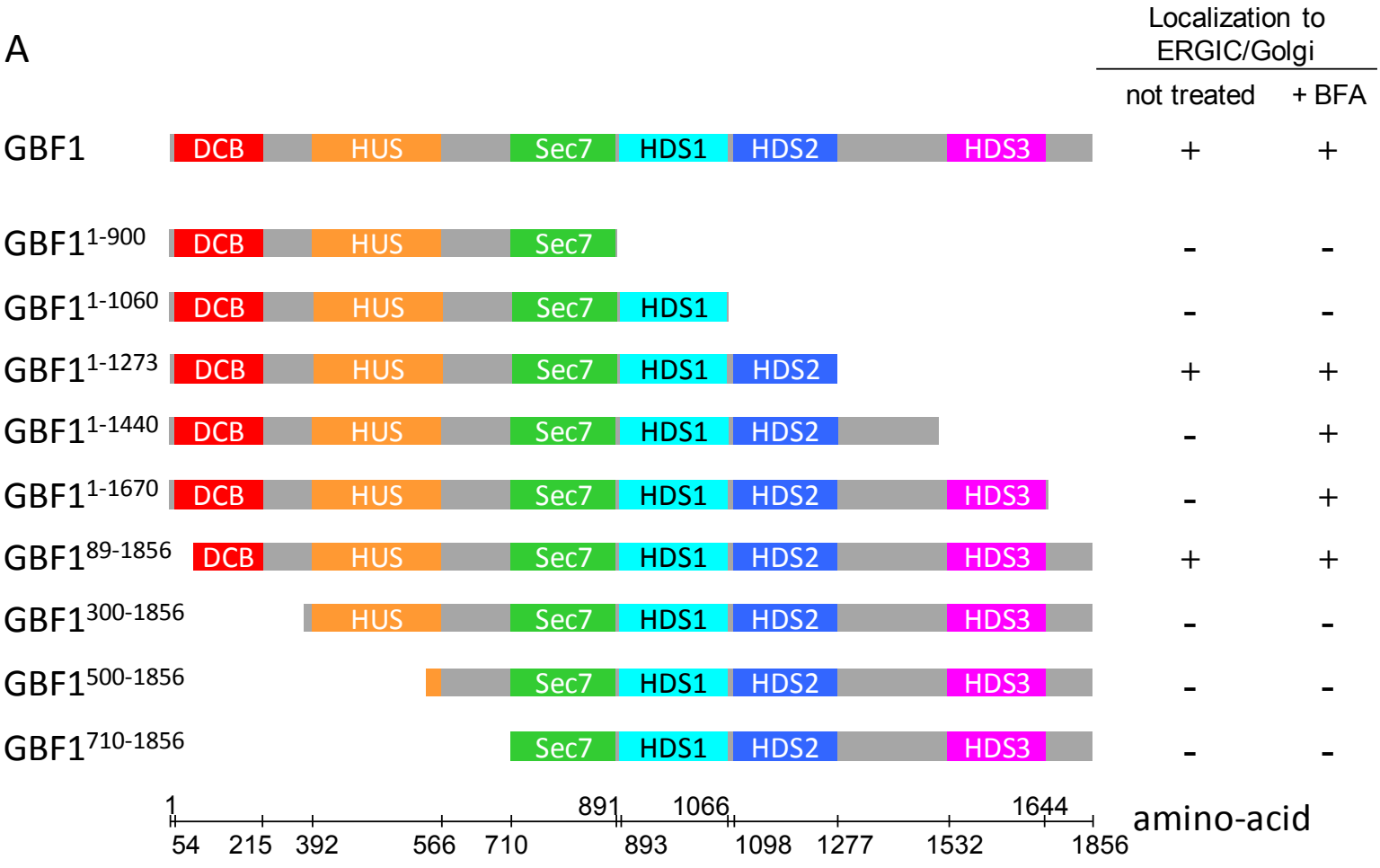
A
Localization to ERGIC/Golgi
not treated
+ BFA
GBF1
DCB
HUS
Sec7
HDS1
HDS2
HDS3
+
+
GBF1 1-900
-
-
GBF1 1-1060
-
-
GBF1 1-1273
+
+
GBF1 1-1440
-
+
GBF1 1-1670
-
+
GBF1 89-1856
+
+
GBF1 300-1856
-
-
GBF1 500-1856
-
-
GBF1 710-1856
-
-
1
891
1066
1644
amino-acid
54
215
392
566
710
893
1098
1277
1532
1856

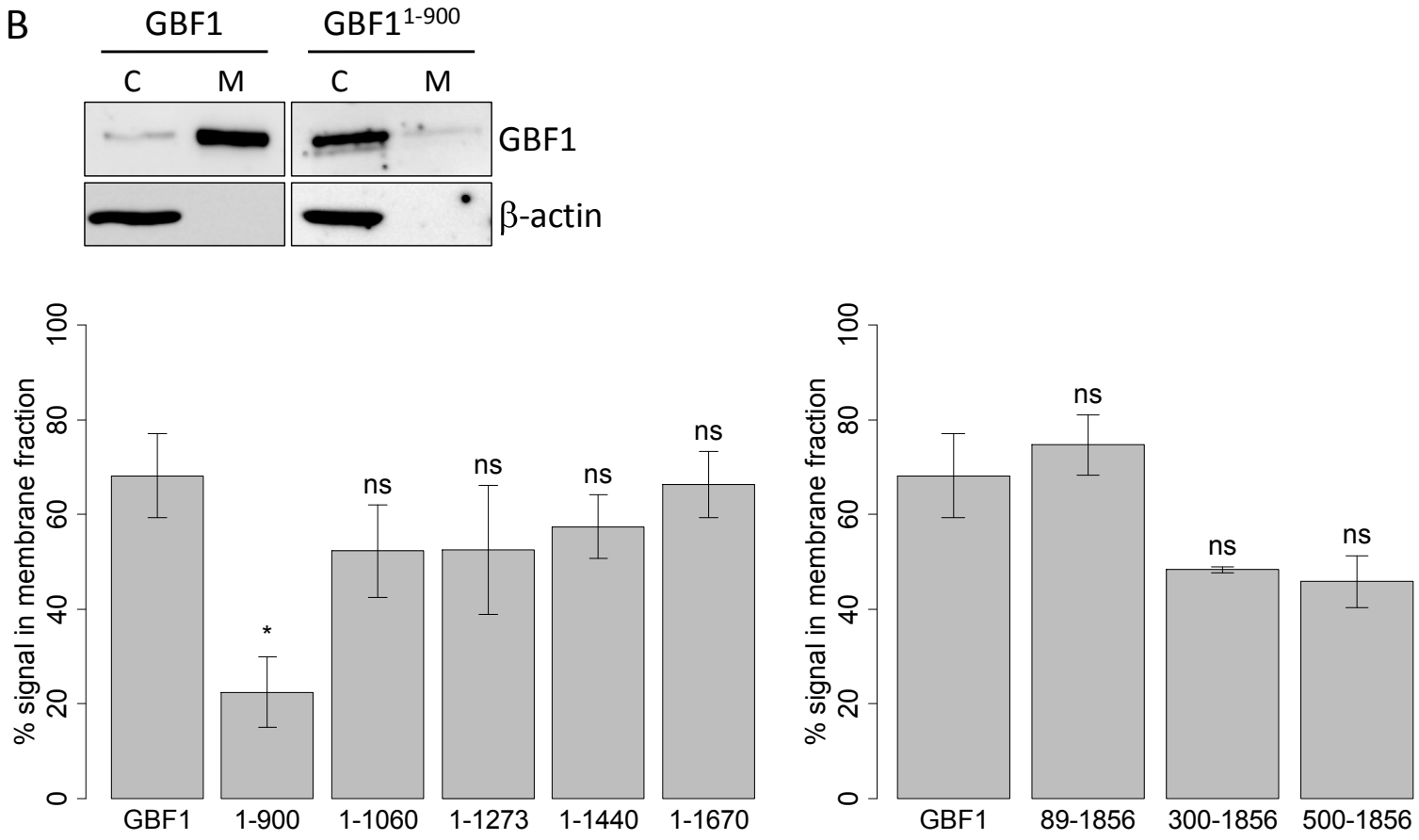
B
GBF1
GBF1 1-900
C
M
C
M
GBF1
β-actin
% signal in membrane fraction
0
20
40
60
80
100
*
ns
GBF1
1-900
1-1060
1-1273
1-1440
1-1670
89-1856
300-1856
500-1856

Figure S3

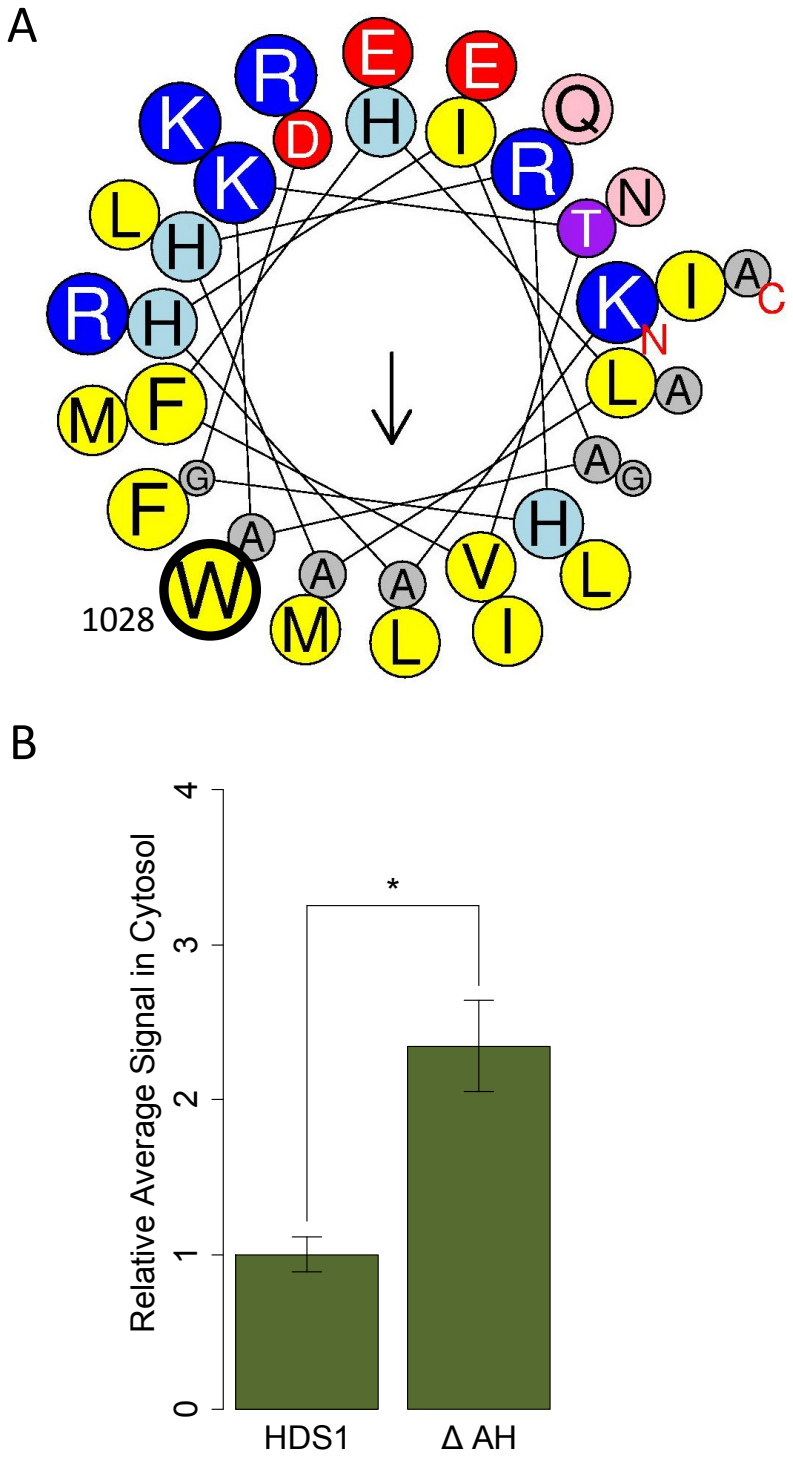
A
R
E
E
K
D
H
I
Q
K
R
N
L
T
H
K
I
A
C
R
H
N
L
A
M
F
A
G
F
G
H
A
V
L
A
A
W
M
L
I
1028
B
Relative Average Signal in Cytosol
0
1
2
3
4
*
HDS1
Δ AH

SUPPLEMENTARY FIGURE LEGENDS

Figure S1: BFA treatment stabilizes the association of overexpressed GFP-GBF1 with membranes. (A) HeLa cells expressing GFP-GBF1 were incubated with 10 µg/mL BFA or DMSO (NT) for 10 min at 37°C before fractionation analysis. Blot shown is representative of 4 independent experiments. C: cytosolic fraction. M: membrane fraction. β-actin: marker of cytosolic fraction. p58: marker of membrane fraction; **(B)** Band density was quantified using Image J software (NIH) and the amount of membrane bound protein was calculated as described in Materials and Methods. Error bars represent the 95% confidence interval. ***p-value $<10^{-6}$ (Standard t-test).

Figure S2: Both the C-terminus and the N-terminus of GBF1 are required for localization to ERGIC and Golgi membranes in cells. (A) HeLa, RPE-1 and/or Cos7 cells expressing the indicated pVenus-GBF1 construction were treated with BFA (+BFA) or DMSO diluent alone (not treated) after overnight incubation and live cell imaging was performed. The Golgi/ERGIC localization (+) is defined as an accumulation of signal in the perinuclear region whereas the cytoplasmic localization (-) corresponds to a diffuse signal throughout the cell; **(B)** Fractionation of cells expressing the indicated GFP-GBF1 construct after treatment with 10 µg/mL BFA for 10 min. Blot shown is representative of 3 independent experiments. C: cytosolic fraction. M: membrane fraction. β-actin: marker of cytosolic fraction. Quantifications shown in the bottom panel were performed as described in Figure 1. Error bars represent the 95% confidence interval. * p-value< 0.001 (Standard Student t-test).

Figure S3: The C-terminal amphipathic region of HDS1 and effects of mutations within this region on HDS1 lipid binding. (A) Helical wheel plot of the predicted C-terminal amphipathic region of HDS1 (GBF1 amino acids 1005-1041) showing the conserved tryptophan (W1028). Calculations of α-helical properties were performed using the Heliquest prediction software (heliquest.ipmc.cnrs.fr/); **(B)** HeLa cells expressing mCherry-HDS1 wild type or with the deletion of the AH shown in Figure 3A, the C-terminal portion of the region shown in part (A) (GBF1 amino acids 1021-1041) were treated with oleic acid before fixing and staining with BODIPY to visualize LDs as described in Figure 3. Quantifications of the association with LDs were performed as described in Materials and Methods. *p-value $<10^{-3}$ (Standard t-test).

Supplemental Table S1. Plasmids used in this study

Plasmid	Expressed protein	Reference
pTKN101	Venus-GBF1(1-1856) (*H. sapiens*)	Jackson laboratory
pVenus-N-GBF1	Venus-GBF1(1-900) (*H. sapiens*)	Jackson laboratory
pVenus-GBF1-1060	Venus-GBF1(1-1060) (*H. sapiens*)	Jackson laboratory
pVenus-GBF1-1273	Venus-GBF1(1-1273) (*H. sapiens*)	Jackson laboratory
pVenus-GBF1-1440	Venus-GBF1(1-1440) (*H. sapiens*)	Jackson laboratory
pVenus-GBF1-1670	Venus-GBF1(1-1670) (*H. sapiens*)	Jackson laboratory
pTKN265	Venus-GBF1(89-1856) (*H. sapiens*)	Jackson laboratory
pTKN900	Venus-GBF1(300-1856) (*H. sapiens*)	Jackson laboratory
pTKN1500	Venus-GBF1(500-1856) (*H. sapiens*)	Jackson laboratory
pVenus-HDS1-GBF1	Venus-GBF1(900-1067) (*H. sapiens*)	Jackson laboratory
pVenus-HDS2-GBF1	Venus-GBF1(1067-1278) (*H. sapiens*)	Jackson laboratory
pVenus-C-GBF1	Venus-GBF1(710-1856) (*H. sapiens*)	Jackson Laboratory
pVenus-GBF1-HUStoHDS2	Venus-GBF1(211-1278) (*H. sapiens*)	This study
pEGFP-GBF1ΔHDS1	GFP-GBF1 with aa 887-1066 deleted (*H. sapiens*)	This study
pEGFP-GBF1ΔHDS2	GFP-GBF1 with aa 1068-1278 deleted (*H. sapiens*)	This study
pEGFP-GBF1ΔHDS1-2	GFP-GBF1 with aa 887-1278 deleted (*H. sapiens*)	This study
pEGFP-GBF1ΔAH	GFP-GBF1with aa 1021-1041 deleted (*H. sapiens*)	This study
pEGFP-GBF1-Sec7-HDS1	GFP-GBF1(710-1066) (*H. sapiens*)	This study
pEYFP-Sec7-GBF1	YFP-GBF1(710-894) (*H. sapiens)*	Jackson laboratory
pEYFP-GBF1ΔSec7	YFP-GBF1 with aa 710-900 deleted (*H. sapiens*)	Jackson laboratory
pEGFP-GBF1-AH	GFP-GBF1(1021-1048) (*H. sapiens*)	This study
pVenus-GBF1-AH	Venus-GBF1(1021-1048) (*H. sapiens*)	This study
pmCherry-C1	mCherry	George Patterson[a]
pmCherry-HDS1-GBF1	mCherry-GBF1(911-1066) (*H. sapiens*)	This study
pmCherry-HDS1-GBF1-I1023K	mCherry-GBF1(911-1066) with the I1023K mutation (*H. sapiens*)	This study
pmCherry-HDS1-GBF1-L1024A	mCherry-GBF1(911-1066) with the L1024A mutation (*H. sapiens*)	This study
pmCherry-HDS1-GBF1-R1025S	mCherry-GBF1(911-1066) with the R1025S mutation (*H. sapiens*)	This study
pmCherry-HDS1-GBF1-W1028S	mCherry-GBF1(911-1066) with the W1028S mutation (*H. sapiens*)	This study
pmCherry-HDS1-GBF1-I1031A	mCherry-GBF1(911-1066) with the I1031A mutation (*H. sapiens*)	This study
pmCherry-HDS1-GBF1-L1038A	mCherry-GBF1(911-1066) with the L1038A mutation (*H. sapiens*)	This study
pmCherry-HDS1-GBF1-R1040S	mCherry-GBF1(911-1066) with the R1040S mutation (*H. sapiens*)	This study
pmCherry-HDS1-GBF1-R1025S-W1028S	mCherry-GBF1(911-1066) with the R1025S and W1028S mutations (*H. sapiens*)	This study

pmCherry-HDS1-GBF1-W1028S-K1029S	mCherry-GBF1(911-1066) with the W1028S and K1029S mutations (*H. sapiens*)	This study
pmCherry-HDS1-GBF1-AAA	mCherry-GBF1(911-1066) with the L1024A, I1031A and L1038A mutations (*H. sapiens*)	This study
pmCherry-GBF1-AH	mCherry-GBF1(1021-1048) (*H. sapiens*)	This study
pmCherry-Sec7-HDS1-GBF1	mCherry-GBF1(710-1066) (*H. sapiens*)	This study
pGEX-4T1-Sec7-GBF1	GST-GBF1(689-895) (*H. sapiens*)	This study
pGEX-4T1-Sec7-HDS1	GST-GBF1(695-1066) (*H. sapiens*)	This study
pGEX-4T1-HDS1-GBF1	GST-GBF1(911-1066) (*H. sapiens*)	This study
pGEX-4T1-HDS1-W1028S-GBF1	GST-GBF1(911-1066) with the W1028S mutation (*H. sapiens*)	This study
pGEX-4T1-HDS1ΔAH -GBF1	GST-GBF1(911-1066) with aa 1021-1041 deleted (*H. sapiens*)	This study
pGEX-4T1-AH-GBF1	GST-GBF1(1005-1048) (*H. sapiens*)	This study
pET11d-Arf1	Arf1 (*Bos taurus*)	Bruno Antonny[b]
pBB(NMT)	N-myristoyltransferase (*S. cerevisiae*)	Bruno Antonny[b]

[a] National Institute of Biomedical Imaging and Bioengineering, NIH, USA
[b] CNRS-Institut de Pharmacologie Moléculaire et Cellulaire, Sophia Antipolis, France